Applied Catalysis B: Environmental 183 (2016) 343–360

Contents lists available at ScienceDirect

Applied Catalysis B: Environmental

journal homepage: www.elsevier.com/locate/apcatb

Pd model catalysts: Effect of aging environment and lean redispersion

Jason A. Lupescu[a,b,*], Johannes W. Schwank[a], Kevin A. Dahlberg[a], Chang Yup Seo[a], Galen B. Fisher[a], Sabrina L. Peczonczyk[b], Kevin Rhodes[b], Mark J. Jagner[b], Larry P. Haack[b]

[a] University of Michigan, Ann Arbor, MI 48109, USA
[b] Ford Motor Company, Dearborn, MI 48124, USA

ARTICLE INFO

Article history:
Received 16 July 2015
Received in revised form
19 September 2015
Accepted 10 October 2015
Available online 30 October 2015

Keywords:
Palladium
Redispersion
TWC
Regeneration

ABSTRACT

The performance of automotive three-way catalysts (TWC) deteriorates with time, temperature and aging environment. Engine control methods are needed to minimize the extent of catalyst deactivation and provide an environment capable of partially redispersing noble metal catalyst particles. In this study, palladium-based model powder catalysts on ceria-zirconia or alumina supports were exposed to three different exhaust compositions, lean-only, rich-only and redox, each at 700 °C for 16 h. Catalyst activity was determined by CO oxidation with the water gas shift (WGS) reaction and oxygen storage capacity (OSC) measurements to probe the contact between the noble metal and support at a given state of catalyst deterioration. Lean catalyst treatments at 550 °C and 700 °C were applied to determine the effect on measured Pd size and catalyst activity. The lean-only gas environment was above the PdO decomposition condition, yet showed slightly deteriorated catalyst activity from the fresh state. The rich-only and redox gas environments significantly deteriorated catalytic activity through a combination of metal oxidation state effects and support/additive interactions, both with various degrees of reversibility depending on lean treatment time and temperature. The insight gained from this work could be used to develop engine control and after treatment design strategies to track (or infer) the aging process on the vehicle, avoid severe aging modes and actively intervene at various points to regenerate the catalyst.

1. Introduction

Automotive manufacturers are required to modify an increasing fraction of their annual production fleet towards meeting extremely low tailpipe emission standards. The catalytic converter together with engine controls for exhaust oxygen management were developed to simultaneously oxidize and reduce three regulated combustion pollutants of carbon monoxide (CO), nitrogen oxides (NOx) and hydrocarbons (HC) [1,2,3]. The current state of this three-way catalyst (TWC) converter washcoat technology contains noble metals (Pt, Pd and/or Rh) impregnated onto a complex support material composed of alumina (Al_2O_3) for high surface area, mixed oxides of ceria and zirconia (CZO) for oxygen storage capacity (OSC) promotion, and rare earth oxides such as lanthana (La_2O_3) to stabilize the alumina surface area. The harsh exhaust gas environment causes the vast initial amount of noble metal to end up buried inside large metal agglomerates and lost to gas-phase reactions [4,5,6]. Characterization studies of full useful life aged automotive TWCs revealed that dispersion of noble metals was only about 1–5% [7,8]. The catalytic converter suppliers must include excessive quantities of expensive noble metals and rare earth oxides to ensure the residual activity after full useful life aging (150,000 miles) is adequate to abate engine emissions. Automotive manufacturers need capable engine controls that avoid or limit the exhaust environments that cause severe TWC deactivation and permit exhaust environments that facilitate restoration of TWC dispersion and function.

Although TWC deactivation is largely irreversible, the catalyst environment can cause a dramatic change in activity and metal dispersion. Hickey et al. subjected Pd model catalysts to either an oxidizing environment (lean aged) or a cycling of reducing and oxidizing environments (redox aged) at 900 °C and showed much less deterioration with the lean aged sample with respect to the temperature required for CO oxidation and the apparent Pd dispersion [9]. Chen et al. aged a series of Pd model catalysts at fixed temperatures in either an oxidizing or reducing environment and showed higher metal dispersion with the samples aged in the oxidizing environment at 850 °C and below [10]. In both works, the samples that were not aged in the oxidizing environment were later exposed

* Corresponding author at: Ford Motor Company, RIC Bldg., MD3179, P.O. Box 2053, Dearborn, MI 48121, USA.
E-mail address: jlupescu@ford.com (J.A. Lupescu).

http://dx.doi.org/10.1016/j.apcatb.2015.10.018
0926-3373/

to oxygen at high temperature and cooled down; further testing and characterization showed a lower temperature for 50% inlet CO conversion and increased Pd dispersion or O_2 uptake compared to the sample that was not exposed to oxygen [9,10]. The cause of this Pd dispersion improvement is linked to earlier observations of PdO migration during heating of Pd/Al_2O_3 catalysts in oxygen and filming them under an electron microscope, where Pd changed to PdO above 325 °C then wet and spread over the support between 350 °C and 800 °C, and finally mobile particles ruptured over the support surface [11,12,13]. Lieske et al. observed that the initial temperature when Pd particles oxidize to PdO was related to the Pd particle size and hence the severity of the catalyst aging [14]. The upper temperature of Pd redispersion was found coincide with PdO decomposition [11,12], which was determined to be a function of the support material and gas phase oxygen concentration [15,16,17]. While oxidized Pd is the prerequisite for Pd redispersion, support collapse and metal-support interaction may limit PdO mobility and particle rupture.

The goals of this investigation were to determine how supported model Pd catalyst characteristics were affected by prolonged exposure to oxidizing and/or reducing exhaust gas environments, and identify opportunities to limit or reverse TWC deactivation that correlate with conditions achievable on a vehicle. The oxygen storage capacity (OSC) and water-gas shift (WGS) tests were included since the oxidation of CO gives insight into activity of the exposed Pd particle surface and contact between the Pd particle and support at a given state of deterioration. Determining the Pd particle size is a challenge because of the various aging mechanisms caused by automotive engine exhaust, the inability of any one characterization technique to give a clear picture of accessible Pd surface sites and the complexity of the materials used in TWC washcoat technology [18,19,20]. We found that the Pd model catalysts were deteriorated most by a redox and constant reducing environment versus exposure to a constant oxidizing environment, but these redox aged catalysts showed improvement in Pd dispersion and catalyst activity test performance after a 700 °C dry air treatment.

2. Experimental

2.1. Preparation of model TWC samples

Pd-based model powder catalysts of 1.5 wt% Pd on La_2O_3-doped γ-Al_2O_3 (Pd/Al) and Pd/ceria-zirconia (Pd/CZO) were prepared at an OEM supplier laboratory by incipient-wetness impregnation of the supports with a palladium solution free from chlorides. After drying, these catalysts were calcined at 500 °C for 4 h in air to fix the metals on the support materials. A mixture was made of the fresh Pd/Al and Pd/CZO model powder catalysts on an equal mass basis to simulate an automotive Pd-based TWC washcoat (Pd/TWC). Two additional samples were acquired for comparison, a 1.6 wt% Pd on TH 100/150 γ-Al_2O_3 without La_2O_3 from Sasol (Pd/A) was described in another work [10] and uncatalyzed $Ce_{0.5}Zr_{0.5}O_2$ (CZO) powder from Solvay. All powders were sieved to obtain particles between 40 and 60 mesh (250–420 microns).

2.2. Model TWC sample aging and lean treatment procedures

Catalyst aging environments were established in a continuous flow reactor at 700 °C for 16 h to simulate in-use drive cycle conditions at the engine-out location. Three aging gas compositions were introduced at a flow rate of 3 L/m: lean-only (0.5% O_2, 10% H_2O and N_2), rich-only (0.75% CO, 0.25% H_2, 10% H_2O and N_2), and redox conditions (alternated 10 min step pulses of lean then rich). Automotive engine operation performs lean/rich switches at a frequency near 1 Hz, but adopting that frequency for our work, the full extreme of each redox pulse may not be sufficiently experienced by the entire depth of powder in the boat. Our conditions were adopted from prior work with quartz boat powder aging in a flow reactor [21]. At 10 min in pulse length, the entire bed of powder was sufficiently exposed to rich and lean environments on each step.

The CO gas stream was scrubbed of iron carbonyls before introduction to the reactor. A 1.50 g portion of catalyst powder was loaded in a quartz boat and placed inside a 19 mm ID quartz reaction tube in the heating zone of the surrounding oven. A thermocouple was placed over the boat in the aging gas stream and a second thermocouple was bent into the boat with the tip buried in the powder. After aging, a few samples were given lean treatments at 550 °C or 700 °C for two hours in 21% O_2/He or zero air to redisperse the sintered Pd particles. Gasoline engines typically operate close to the fuel/air stoichiometric ratio so the automotive catalyst OSC state is generally partly depleted. The catalyst samples in this work were characterized and evaluated in the reduced state by exposing them to a flow of 9% H_2 in argon at 300 °C for 30 min prior to cooling in argon to room temperature.

2.3. Catalyst characterization techniques

The Pd/Al and Pd/CZO catalysts bulk composition was confirmed by X-ray fluorescence (XRF) while the support phase identification was performed with X-ray diffraction (XRD) pattern analysis. The elemental composition was determined using a Philips PW2400 XRF Spectrometer and UniQuant5 software. A catalyst sample mass of 0.7 g on top of 4.5 g of boric acid in aluminum caps were compacted into pellets with a hydraulic press. Pd was quantified using the Lα1 X-ray line. Support phase identification was performed with a Rigaku Miniflex II diffractometer with Cu Kα X-Ray (λ = 1.5406 Å) radiation source set at 30 kV and 15 mA. A catalyst sample mass of 0.1 g was wet-milled with a mortar and pestle in ethanol then dripped onto an off-axis cut silicon crystal sample substrate and dried. Scans were performed with a step size of 0.005°2θ at a scan speed of 1°2θ/min from 5°2θ to 90°2θ.

The surface characteristics of the catalysts were determined by N_2 physisorption and X-ray photoelectron spectroscopy (XPS). The BET specific surface area and BJH pore volume (for pores between 17 and 300 Å) were determined with a Micromeritics ASAP2420 instrument using N_2 adsorption at 77K. A 48-point adsorption and 33-point desorption isotherm plot was generated across a range of 0.1–0.9 P/P_0. Elemental composition and chemical state information were determined with a Kratos AXIS 165 Electron Spectrometer using a monochromatic Al Kα (1486.6 eV) X-ray excitation source operated at 12 kV, 20 mA (240 W). Each sample was pressed into a pellet and then mounted onto sticky double sided pressure sensitive adhesive tape. Data was collected using pass energies of 80 eV or 20 eV to collect survey or high resolution spectra, respectively. All spectra were acquired using charge neutralization with an electron flood source. Elemental quantification of the high resolution spectra was accomplished using CASAXPS software Version 2.3.16, using routines based on Scofield photoionization cross-section values. A Shirley type background was used to fit all high resolution spectra. For Pd on alumina support the high resolution Pd 3d spectra was fit with a doublet using 60% Gaussian and 40% Lorentzian line shapes with an area ratio of 0.667, a full width at half-maximum (FWHM) constrained within 0.6–2.8, and a peak separation of 5.2 eV. For Pd on CZO support, the Zr 3p fit was first determined from a CZO standard using 60% Gaussian and 40% Lorentzian line shapes with an area ratio of 0.5, a FWHM constrained between 0.6 and 2.8, and a peak separation of 13.4 eV. The remaining area under the envelope was then fit by adding Pd 3d peaks using the fitting parameters described above for Pd on alumina. Binding energies were referenced to the aliphatic C 1s peak at 284.6 eV [22].

Pd particle size estimates were performed using three techniques. Post-process curve fitting of the XRD pattern Pd peak for mean Pd crystalline length was performed with the Rigaku PDXL software program. The software calculations used for estimating mean Pd crystalline length from XRD pattern line broadening was based on the Scherrer equation [23]. The shape factor used was 0.89 for spherical crystallites and the peak integral method was used to determine peak breadth. The instrument broadening was corrected with a LaB_6 calibration standard. H_2 chemisorption was performed using a Micromeritics ASAP2020 instrument with a static volumetric adsorption/out-gas/re-adsorption method described by Chen et al. [10]. Prior to analysis, each sample was first degassed in N_2 at 500 °C, reduced at 350 °C in pure H_2, exposed to vacuum at 1 microtorr and finally dosed with H_2 at 35 °C for chemisorption measurements using a 5-point isotherm extrapolated to zero pressure. This technique is an improvement upon the classic H_2–O_2 titration method and avoids problems of H_2 spill-over and Pd hydride formation from interfering with the irreversible adsorbed H_2 calculation [24,25]. The differential results were used to report Pd dispersion and size to exclude physisorbed H_2 on the support. H_2 chemisorption was used for all samples since we found that CO chemisorption significantly overestimated the Pd dispersion on the CZO supports, probably due in part to CO adsorption on CZO forming stable carbonate species [26]. Scanning transmission electron microscope (STEM) images were collected with a JEOL 2010F instrument using high angle annular dark-field (HAADF) imaging. The microscope was equipped with a zirconated tungsten [100] thermal field emission tip filament and operated at 1.5×10^{-7} torr vacuum with 200 kV accelerating voltage. The JEOL HAADF detector had a probe size of 0.5 nm and camera length of 12 cm. Samples for imaging were prepared by dispersing 10 mg of catalyst sample powder in 2 mL of ethanol followed by ultrasonification for one hour to make a suspension, then dripped onto a 200-mesh carbon coated copper grid and dried. The Pd particle diameter was calculated with Image J software. A JEOL 3100R05 Double Cs-Corrected analytical electron microscope with a resolution of 0.055 nm point-to-point was used to image Pd/CZO samples. However, even with this powerful instrument, we were unable to discern Pd on CZO due to the poor diffraction contrast between Pd and the CZO support. Furthermore, electron beam heating caused rapid growth of carbonaceous overlayers obscuring the image and hindering elemental mapping by energy-dispersive X-ray spectroscopy. After removal of these carbonaceous overlayers in a heated sample stage, charging induced image artifacts made it impossible to reach the required resolution.

2.4. Catalyst activity measurements

A flow reactor was used to enable measurement of CO_2 formed by probe reaction tests on a characterized catalyst sample. The ASAP2020 quartz j-tube and sample used in the H_2 chemisorption test was fit onto the flow reactor. The j-tube measured 10.5 mm ID and a catalyst sample mass of 0.30 g was loaded between 6 mm redistributing layers of quartz wool. The bed height was 4 mm for the Pd/CZO and 6 mm for Pd/Al samples. Matheson dynablenders and flow controllers managed the gas flow through the system. The gas stream could be triggered to route through a water bubbler and lines were maintained at 150 °C to limit condensation. The CO gas stream was scrubbed of iron carbonyls with alumina chips heated at 350 °C. Two K-type 1/32-inch diameter thermocouples were placed 16 mm before and 13 mm after the sample bed. A Hiden HPR20 quadrupole electron ionization mass spectrometer with secondary electron multiplier (SEM) detector measured five mass values in torr with a 2 Hz sampling rate at an inlet sampling pressure of 1E-5 torr and required two corrections to normalize the signals from other species into individual concentrations. First, the double excitation argon (Ar) mass 20 value was scanned, which is 11% of the total Ar level, rather than the typical mass 40 to get the measured Ar value below the SEM detector limit of 1×10^{-6} torr. Second, there was a CO and CO_2 mass overlap of 11.4%, so that amount of the CO_2 value was subtracted from the CO value. OSC measurements were run by alternating one minute lean or rich pulses, each separated by a one minute purge. The purge pulse was CO_2 and Ar at 975 mL/min while a square step pulse of CO in Ar or O_2 in Ar was added at 25 mL/min. The lean pulse was 1% O_2, 2% CO_2 and balance Ar. The rich pulse was 2% CO, 2% CO_2 and balance Ar. At least five CO pulses were measured in each 50 °C increment, starting at 50 °C and ending at 400 °C. WGS measurements were run with a constant feed of 2% CO, 2% CO_2, 2.5% H_2O and Ar at 1 L/min. The gas mixture was initially established at equilibrium over the catalyst sample at 50 °C, then the oven heating ramp was triggered at 10 °C/min to 400 °C.

Table 1
Characterization of fresh sample elemental oxide compositions by XRF.

Pd/Al	Pd/CZO
93.7 wt% Al_2O_3	54.7 wt% CeO_2
3.86 wt% La_2O_3	42.4 wt% ZrO_2
1.42 wt% Pd	1.42 wt% Pd
0.40 wt% Pr_6O_{11}	0.80 wt% HfO_2
0.30 wt% SO_3	0.49 wt% Al_2O_3
0.05 wt% CaO	0.10 wt% La_2O_3
0.27 wt% other	0.09 wt% other

2.5. Vehicle TWC emission and temperature evaluation

The Ford Motor Company vehicle emission research laboratory (VERL) evaluated a 2009MY 2.0L Ford Focus test vehicle with gasoline fuel. Only the front tires were in contact with the exposed dynamometer roll surface that simulated EPA certification road conditions. The vehicle was operated using the light-duty vehicle FTP-75 (federal test procedure) and US06 Supplemental Federal Test Procedure (SFTP). Tailpipe emissions were measured using Horiba MEXA 9000 analyzers at a 1 Hz data collection rate and the exhaust emissions and fuel parameters were used to calculate the engine exhaust lambda equivalence ratio, or the actual air/fuel ratio divided by the stoichiometric air/fuel ratio, by the Spindt method [27]. K-type thermocouples were installed through-out the exhaust system including one in the catalytic converter bed location, which was 1 inch downstream of the first brick front face.

3. Results

3.1. Sample composition characterization and aging comparison

The XRF elemental oxide composition results of the Pd model catalysts are shown in Table 1. Concentrations were calculated as oxides (except Pd, which was calculated as an element). Reported values of just the top components are listed in weight percent since minor amounts of other species were also detected in the catalyst sample. The catalysts contained the same amount of Pd metal. The Pd/Al catalyst contained about 94% alumina with about 4 wt% lanthana added for surface area stabilization against steam. The 0.4 wt% Pr_6O_{11} in the aluminum support was considered an impurity of the lanthana. The Pd/CZO catalyst contained primarily ceria and zirconia oxide in a weight ratio of 56/44 and atomic ratio of 50/50. The 0.8 wt% HfO_2 was considered an impurity of zirconia.

The conditions used to age these catalyst samples were compared to the literature. Peuckert developed an equation for the temperature of bulk PdO decomposition as a function of gas phase oxygen concentration [16]. Fig. 1 shows a plot of that equation for a pressure of 1 atm. Lieske and Völter observed that Pd needed

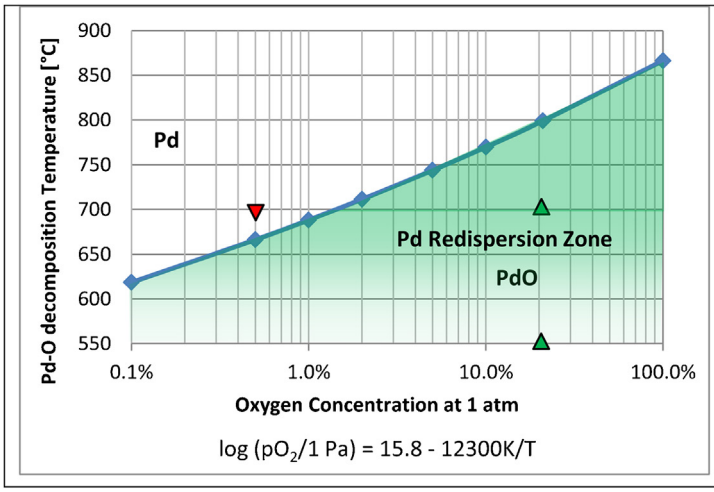

pO_2 at a basis of 1 atm	Bulk PdO Decomposition Temperature (°C)
0.5%	670°C
21%	800°C

Key	Condition
▼	Redox aging (lean step)
▲	Lean Pd regeneration

Fig. 1. Palladium oxide thermal stability from reference [16].

to be oxidized before redispersion would occur [14], so the "Pd Redispersion Zone" shown in Fig. 1 must extend below the PdO decomposition line. The lean-only and lean redox step at 700 °C used just 0.5% O_2, an environment where the catalyst was above the bulk PdO decomposition temperature of about 670 °C. Colussi et al. ran heating/cooling cycles in 0.5% O_2 and observed a similar 677 °C onset temperature of PdO decomposition when supported on either Al_2O_3 or 10% CeO_2–Al_2O_3, however the PdO reformation temperature began near 600 °C on 10% CeO_2–Al_2O_3 and near 500 °C on Al_2O_3 [17]. Therefore, once the PdO on our catalysts decomposed into Pd near 670 °C during heating in 0.5% O_2 up to 700 °C, reoxidation of Pd would not occur until the temperature had dropped below the hysteresis temperature. Consequently, the supported Pd would likely be in the metallic state for all three aging environments. The lower Pd redispersion zone boundary was tested with lean treatments at 550 °C or 700 °C in dry air, an environment where the supported catalyst was well below the bulk PdO decomposition temperature of about 800 °C. These lean treatment conditions were based on work by Chen et al. who demonstrated higher Pd dispersion when the lean feed gas stream was dry compared to one containing 10% steam [10].

3.2. Surface area and pore volume characterization

The BET surface area and BJH adsorption pore volume for each sample are listed in Table 2, both fresh and after exposure to various aging environments. The fresh Pd/Al sample had a surface area of 209 m^2/g and a pore volume of 0.58 cm^3/g. The 700 °C/16 h lean aged Pd/Al sample showed a decrease of about 20% in surface area and about 7% in pore volume, relative to the fresh Pd/Al sample. All of the aged Pd/Al samples had a surface area within 3% of 160 m^2/g and the pore volume within 2% of 0.54 cm^3/g, which demonstrated an insensitivity of the alumina to the aging environments. The fresh Pd/CZO sample had a surface area of 91 m^2/g and a pore volume of 0.16 cm^3/g. The 700 °C/16 h lean aged Pd/CZO sample showed a decrease of about 46% in surface area and 6% in pore volume relative to the fresh Pd/CZO sample. The redox aging method was the most severe for the Pd/CZO samples with a 62% surface area loss compared to loss of 55% for rich-only and 46% for lean-only. Unlike alumina, CZO is a reducible support under these conditions and the repeated redox cycling was more degrading to CZO than the constant rich-only environment after 16 h. The Pd/TWC sample had a surface area and pore volume in between that of the Pd/Al and Pd/CZO samples. The lean treatments of 550 °C/2 h or 700 °C/2 h in air showed minor effects on the surface area or pore volume. The fresh Pd/A sample had a surface area of 138 m^2/g and a pore volume of 0.75 cm^3/g. The 700 °C/16 redox aged Pd/A sample showed a decrease of about 10% in surface area and no loss of pore volume relative to the fresh Pd/A sample. The fresh Pd/A sample had about 30% lower surface area, but about 20% higher pore volume than the fresh Pd/Al sample. The fresh CZO sample had similar surface area, but over twice the pore volume than the fresh Pd/CZO sample.

3.3. Pd particle size characterizations

Three techniques were used to assess the changes to the Pd particle size from the fresh to aged state, since each had limitations. The XRD peak analysis provides a quantitative volumetric bulk estimate of the Pd crystallite size, unless the Pd particles are agglomerated crystallites, or a large number of the Pd particles are small (<7 nm) and undetectable apart from the background XRD pattern. H_2 chemisorption provides a quantitative measurement of exposed metal surface, but strong metal-support interactions reduce probe molecule adsorption [18,19] and yield overly large calculated Pd particle sizes. The STEM image was assumed to contain spherical shapes to calculate the Pd particle diameter. Imaging the Pd particles on CZO samples proved too difficult since electron microscopy provides little contrast between small metallic Pd particles and a CeO_2 support [20].

The bulk Pd metal dispersion (D) is related to the bulk Pd particle size (d_p), assuming spherical shapes, by the following equation used by Baylet et al. [28]:

$$D[\%] = \frac{\left(6 \times 10^5\right) \times (M_{Pd})}{\left(\rho_{Pd} \times S_{Pd} \times d_p\,[nm]\right)}$$

With M_{Pd} as the palladium molar weight of 106.4 g/mol, ρ_{Pd} as the palladium density of 12 g/cm^3, S_{Pd} as the molar surface area of palladium assuming an equidistribution of the low index faces of 47,780 m^2/mol for Pd metal.

3.3.1. XRD pattern phase identification

The XRD patterns of the fresh, aged and post lean treated samples of Pd/Al are shown in Fig. 2a and are consistent with gamma alumina support material. The XRD patterns of the fresh, aged and post lean treated samples of Pd/CZO are shown in Fig. 2b and are consistent with the expected peaks for CZO support. No new support phases were observed during the 700 °C aging for either model catalyst. The redox aged Pd/CZO sample had a small peak emerge at 26.4°2θ, which could be the cubic phase of Ce_2O_3 [100] and indi-

Table 2
Characterization of fresh and aged catalyst samples.

Sample	Condition	Surface area [m^2/g]	Pore volume [cm^3/g]	Pd dispersion [%]		Pd particle size [nm]	
				by H_2[a]	by XRD[b]	by H_2[a]	by XRD[b]
Pd/Al	Fresh	209	0.58	9.1%	7.9%	12	14
	Lean-only 700 °C/16 h	164	0.54	5.0%	5.9%	22	19
	Rich-only 700 °C/16 h	158	0.54	1.0%	6.8%	107	16
	+550 °C/2 h air	157	0.53	4.6%	7.5%	24	15
	Redox (10/10) 700 °C/16 h	164	0.55	0.7%	6.8%	159	16
	+550 °C/2 h air	161	0.54	3.9%	7.3%	28	15
	+700 °C/2 h air	157	0.53	5.7%	7.6%	19	14
Pd/CZO	Fresh	91	0.16	22%	u/d	4.9	u/d
	Lean-only 700 °C/16 h	49	0.15	15%	u/d	7.3	u/d
	Rich-only 700 °C/16h	41	0.15	u/d	10%	u/d	11
	+550 °C/2 h air	41	0.15	0.8%	10%	134	11
	Redox (10/10) 700 °C/16 h	35	0.15	u/d	5.6%	u/d	20
	+550 °C/2 h air	35	0.15	u/d	5.4%	u/d	20
	+700 °C/2 h air	35	0.15	4.1%	4.5%	27	24
Pd/TWC	Fresh	138	0.34	12%	14%	9.2	7.8
	Redox (10/10) 700 °C/16 h	94	0.33	u/d	8.7%	u/d	13
	+550 °C/2 h air	97	0.35	2.3%	7.4%	49	15
	+700 °C/2 h air	90	0.33	4.9%	8.2%	23	13
Pd/A	Fresh	138	0.75	10%	11%	11	10
	Redox (10/10) 700 °C/16 h	124	0.80	5.0%	7.4%	22	15
CZO	Fresh	97	0.46	–	–	–	–

[a] H_2 Chemisorption by difference method.
[b] XRD Pd peak fit by Scherrer equation.

cate an aging induced phase separation out of bulk CZO [29,30,31], but the accompanying peak of Ce_2O_3 [101] at 30.3°2θ is not in the pattern, so this peak at 26.4°2θ is the K(β) reflection of CZO [111]. The Pd metal peak was observed at 40°2θ only for the redox and rich-only aged Pd/CZO samples. The fresh and lean-only aged CZO samples had Pd particles that were too small to be detected by XRD. The XRD patterns of the combined Pd/TWC sample are shown in Fig. 2c with every Pd peak at least partially confounded by a support peak. The Pd peak used to obtain line broadening or peak width measurements for particle size determination was 40°2θ [111] on the Pd/CZO and Pd/TWC samples, and 82°2θ [311] on the Pd/Al samples.

3.3.2. *Average Pd size estimation comparison with H_2 chemisorption and XRD*

The apparent Pd dispersion and Pd particle size for each sample are listed in Table 2. Some conditions resulted in undetectable (u/d) Pd size measurements. The Pd metal sintering severity as measured by XRD was similar for each aging environment on the Pd/Al samples, but had a clear trend with environment on the Pd/CZO samples with redox (20 nm) > rich-only (11 nm) > lean-only (u/d). These Pd/Al size results seem to conflict with the results of Chen et al. on Pd/Al_2O_3 or Kang et al. on Pd/TWC that showed much more severe Pd dispersion loss with rich aging than lean aging in the temperature range of 600 °C–700 °C [10,32], however their lean aging feed included 3% O_2 or more that maintained the Pd in the oxidized state to prevent sintering while the 0.5% O_2 used in our lean aging feed fell below the Pd–PdO transition conditions shown in Fig. 1. Large discrepancies in rich-only and redox aged sample Pd dispersion results between H_2 chemisorption and XRD methods in Table 2 may indicate that the support material chemically affected the Pd particles, partially encapsulated the Pd particles or decorated the Pd surface, which are all examples of strong metal support interaction (SMSI) [18,19,20,33,34,35,36,37,38].

The lean treatment at 550 °C or 700 °C had different effects on the Pd particle sizes listed in Table 2 depending on the support material and aging environment. The lean treatment of 550 °C/2 h showed minor improvements in Pd dispersion as measured by H_2 chemisorption, but the redox aged Pd/CZO sample stayed undetectable. The Pd size measured by XRD appeared to confirm that the lean treatment of 550 °C/2 h had a minor reduction for the redox and rich-only aged Pd/Al samples, while showing no change for the Pd/CZO samples. The lean treatment of 700 °C/2 h on the redox aged Pd/Al sample increased Pd dispersion from 0.7% to 5.7% as measured by H_2 chemisorption, which appeared to be confirmed by XRD with a reduction of 2 nm in the bulk Pd crystallite size. The lean treatment of 700 °C/2 h on the redox aged Pd/Al sample produced Pd particles that were comparable in size to the lean-only aged Pd/Al sample as measured by H_2 chemisorption. The lean treatment of 700 °C/2 h on the redox aged Pd/CZO sample increased Pd dispersion from u/d to 4.1% as measured by H_2 chemisorption, but a bulk Pd crystallite size reduction was not confirmed by XRD. With both lean treatments, H_2 chemisorption and XRD Pd peak fitting methods suggest that Pd redispersion occurred on the redox aged Pd/Al samples, while both methods did not agree that Pd redispersion occurred on the Pd/CZO samples. The 700 °C lean treatment demonstrated better Pd redispersion results than the 550 °C lean treatment.

3.3.3. *STEM image*

The STEM images for fresh and redox aged Pd/Al samples are shown in Fig. 3. The Pd particles shown in the dark field are bright and appear to be roughly circular in shape given the 2D image. Fig. 3a shows the small Pd particles in the fresh condition while Fig. 3b shows much larger Pd particles after redox aging at 700 °C for 16 h. Fig. 3c shows the Pd particles size and shape after the lean treatment at 550 °C for 2 h lacked the large crystals compared to before the lean treatment in Fig. 3b. Fig. 3d shows the Pd particles size and shape after the lean treatment at 700 °C for 2 h are smaller compared to before the lean treatment in Fig. 3b. In addition, Fig. 3d shows Pd particles with "hollow" centers, perhaps due to the presence of a void space at the core, as has been reported elsewhere for Pd metallic particles that were oxidized and then reduced [39,40,41]. Other works with high temperature oxidation of Ni and Co metallic particles, suggest that this void formation was caused by a diffusion couple between metal cations and anions where an inward flux of vacancies towards the particle core was required to offset the flux of faster cations towards the particle surface [42,43]. This process, also known as the nanoscale Kirkendall effect, eventually generates hollow metal particles when the concentration of vacancies at the core is sufficient to coalesce into a single large void

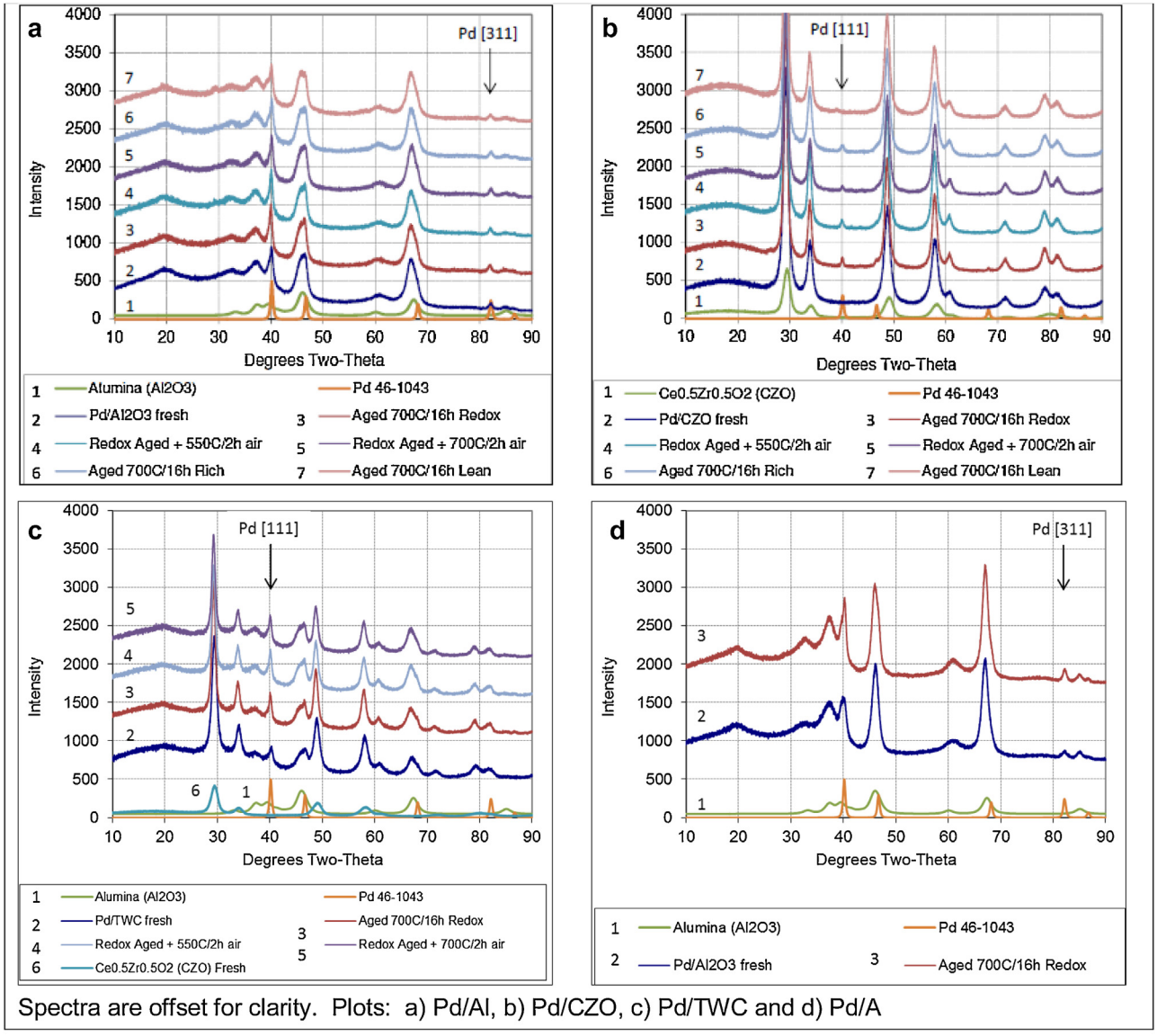

Fig. 2. Pd supported samples X-ray diffraction patterns.

[43]. We attempted acquiring HRTEM images to prove direct evidence of a reducible ceria oxide thin film covering on Pd, but were ultimately unsuccessful at discerning Pd from CZO.

The counted Pd particles are shown as histograms in Fig. 4 with the number average Pd particle size with 99% confidence interval on the mean. The histogram x-axis bins are labeled at the maximum value in the bin range. For example 15 nm is the counted particles in the 11–15 nm range. The aged samples particle size distribution (PSD) each followed a bell shaped curve or normal distribution; except for the fresh PSD that had a long tail of large particles. Therefore, a statistical analysis is applicable for the aged catalysts. A confidence interval contains a set of plausible values for a parameter, such as a mean. A confidence interval equals a theoretical probability point of normally distributed data at critical point α with n-1 degrees of freedom ($t\alpha_{/2,n-1}$), times the standard deviation of the data set (s), divided by the square root of the number of counted particles (n): [44].

$$\mathrm{CI} = \frac{(t_{\alpha/2,n-1}) \times (s)}{\mathrm{SQRT}(n)}$$

A statistical evaluation of Pd redispersion is done by comparing one mean and examining if it is outside the confidence interval around another mean. The fresh sample Pd particles in Fig. 4a had a numerical mean diameter of 6.0 nm +/− 0.7 nm, showing most of the particles in the small range up to 10 nm and a long particle size distribution tail greater than 25 nm. After the 700 °C/16 h redox aging, the sintered Pd particles in Fig. 4b had a numerical mean diameter of 16.0 nm +/− 1.3 nm. The redox aged particles had a tail of "small" particles up to 10 nm making up 18% of the cumulative total and a tail of "large" particles greater than 25 nm making up 5% of the cumulative total. The 550 °C/2 h lean treatment in Fig. 4c produced a numerical mean of 14.6 nm +/− 1.2 nm; a statistically significant reduction in Pd size of 1.4 nm. The tails of small (up to 10 nm) Pd particles were 17% of the cumulative total, essentially unchanged from before the 550 °C/2 h lean treatment. The cumulative total of large (>25 nm) Pd particles decreased to 1%, a reduction from 5%. Therefore at 550 °C in air, the extent of Pd redispersion did not generate new small particles, but shrank the particles greater than 15 nm, increasing the count of particles measuring 11–15 nm from 36% to 43% of the total. The 700 °C/2 h lean treatment in Fig. 4d produced a numerical mean of 11.6 nm +/− 0.7 nm; a statistically

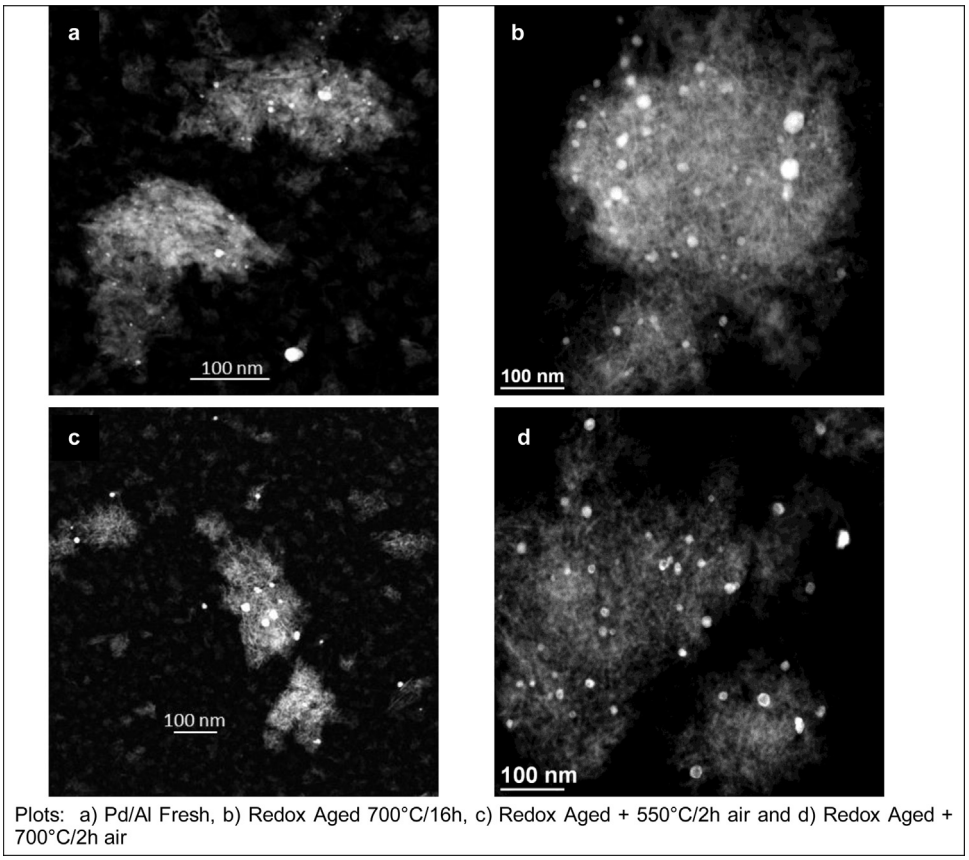

Fig. 3. Pd/Al samples imaged with HAADF STEM.

significant reduction in Pd size of 4.4 nm. The tails of small (up to 10 nm) Pd particles were 34% of the cumulative total, up from 18% before the 700 °C/2 h lean treatment. The cumulative total of large (>25 nm) Pd particles decreased to 0%, a reduction from 5%.

The STEM images of metal particles with diameter, d_i, and the number of particles of a particular diameter, n_i, can be calculated as a surface-averaged diameter to compare against H_2 chemisorption results and a volume-averaged diameter to compare against XRD results as shown by the equations below used by Adams et al. [45]:

$$\underset{d_n = \frac{\Sigma n_i d_i}{\Sigma n_i}}{\text{Number} - \text{average}} \qquad \underset{d_s = \frac{\Sigma n_i d_i^3}{\Sigma n_i d_i^2}}{\text{Surface} - \text{average}} \qquad \underset{d_v = \frac{\Sigma n_i d_i^4}{\Sigma n_i d_i^3}}{\text{Volume} - \text{average}}$$

The resulting STEM number average, surface average and volume average Pd particle size results are shown in Table 3 for fresh and redox aged Pd/Al samples. The Pd particle size measurement from surface averaged STEM and H_2 chemisorption were comparable for all samples except the 700 °C/16 h redox aged sample, likely due to strong metal-support interaction with La_2O_3, which is known to interact with Pd and reduce H_2 adsorption strength [19]. The Pd particle size determined from volume average STEM and XRD were comparable for the fresh and 700 °C/2 h air treatment sample, but were at least twice the Pd crystallite length determined from XRD for the other samples, indicating that some Pd particles in Fig. 3 may have been agglomerates of two or more Pd crystals. The STEM Pd size results listed in Table 3 confirm the Pd size reduction results reported in Table 2 on the redox aged Pd/Al sample after 700 °C/2 h air treatment and to a lesser degree the 550 °C/2 h air treatment.

3.4. XPS surface characterization

The atomic surface concentrations of the top surface layers are shown in Table 4. For the Pd/Al and Pd/A samples, the amount of Pd stayed the same for both fresh and redox aged. This consistency of exposed Pd surface from fresh to aged agrees with the XRD measurements in Table 2 where the Pd size increased from 14 nm to only 16 nm after redox aging on Pd/Al and from 10 nm to just 15 nm after aging on Pd/A. These Pd sizes are well within the detection depth of the XPS instrument. These XPS results also do not show the dramatic drop in Pd dispersion that the H_2 chemisorption results showed for the redox aged Pd/Al sample. The Pd/Al sample showed that surface La increased by 50% from fresh to aged, yet surface Pd stayed about the same, which does not support the proposed model of reduced La_2O_3 species decorating the Pd particle during reducing aging conditions as proposed by Bell et al. [19,46,47]. The increase in La_2O_3 while maintaining similar Pd surface concentra-

Table 3
Comparison of Pd particle diameter measured with STEM to other methods.

Pd/Al samples	Particles counted, n	Number-average, d_n [nm]	Surface-average, d_s [nm]	H_2 chemisorption [nm]	Volume-average, d_v [nm]	XRD [nm]
Fresh	274	6	15	12	22	14
Redox 700 °C/16 h	248	16	27	159	36	16
+550 °C/2 h air	174	15	22	28	30	15
+700 °C/2 h air	204	12	14	19	15	14

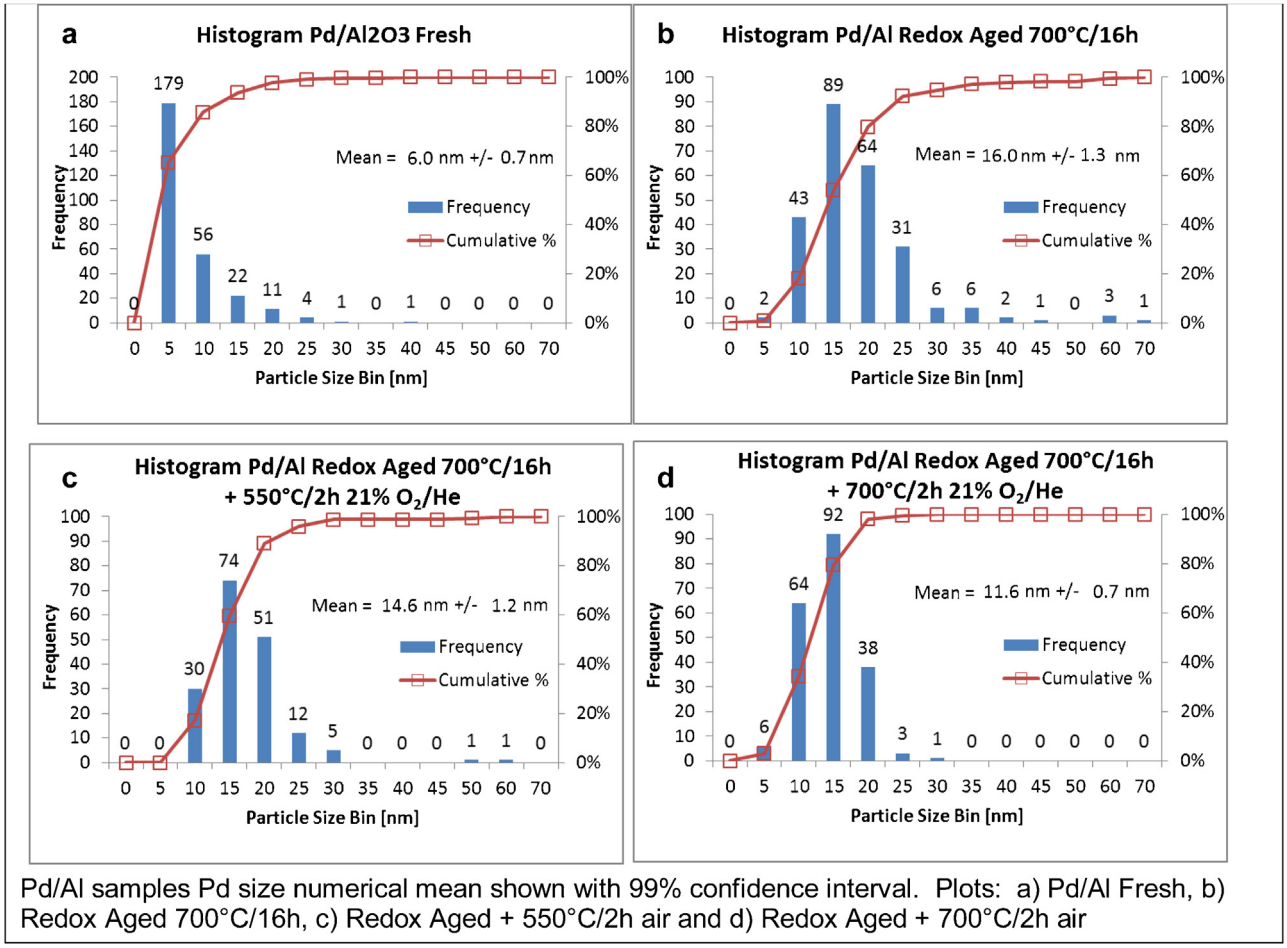

Fig. 4. Pd particle size histograms based on STEM Images of Pd/Al samples.

tions after aging could be explained by: (1) sintering of the alumina surface area leaving more La_2O_3 at the surface, coupled with (2) a phase segregation caused by reducing conditions, which drove more La_2O_3 to the surface that could then interface with the Pd particles. The latter explanation may cause the Pd to exhibit gas phase adsorption characteristics as if supported on La_2O_3 rather than on alumina. For the Pd/CZO catalyst, redox aging decreased the surface concentration of Pd by half simultaneously with a surface concentration increase in Ce by 30% and Zr by 10%, without a significant increase in oxygen. The XRD measurements in Table 2 showed the Pd size increased from less than 7 nm (u/d) to 20 nm after redox aging on Pd/CZO, which was larger than observed on alumina. The loss of half the initial surface Pd atoms from XPS detection coupled with increased surface Ce and Zr atoms was partially due to increased particle size and may also confirm that the reduced support crept up the sides or decorated the Pd surface during redox aging. The increase in surface atoms of Ce was three times the increase in Zr, which is beyond the 50/50 atomic ratio of the support and may be explained by a localized phase separation of CZO where reducible Ce oxide species decorated the Pd surface leaving behind a support richer in ZrO_2. All samples had some adventitious carbon on the surface due to exposure to air and the CZO support material attracted more than the alumina.

The XPS spectra of the Pd/A and Pd/Al catalyst samples are shown in Fig. 5, plots a–c. The Pd/Al sample had a Pd $3d_{5/2}$ peak appear at 334.8 eV +/− 0.1 eV for both fresh and aged conditions that corresponds to the metallic state, plus the fresh Pd/Al sample had a shoulder at about 336.5 eV for Pd^{+2} perhaps due to Pd interface sites with the support La_2O_3. These results are comparable to XPS work reported by Zhao et al. on fresh, reduced 1.4 wt% Pd on La_2O_3-Al_2O_3 support that had the Pd $3d_{5/2}$ peak at 335.2 eV for metallic Pd with a shoulder at 336.5 eV for Pd^{+2} [48]. The Pd/Al sample metallic Pd peak location was shifted below the value reported by Zhao et al. by 0.7 eV. The Pd/A sample had a Pd $3d_{5/2}$ peak appear at 334.5 eV +/− 0.1 eV for both fresh and aged conditions that corresponds to the metallic state, but did not show a peak for Pd^{+2}. Pd catalysts exposed to a high temperature reduction in hydrogen have been reported to show a chemical shift or reduced peak inten-

Table 4
XPS surface elemental composition: atomic percent (at%).

Sample	C	O	Pd	Ce	Zr	Al	La	Pr
Pd/Al Fresh	13.5	48.5	0.22	–	–	37.6	0.20	0.02
Pd/Al Redox 700 °C/16 h	11.7	49.9	0.23	–	–	37.8	0.30	0.01
Pd/A Fresh	11.8	48.7	0.24	–	–	39.3	–	–
Pd/A Redox 700 °C/16 h	12.0	48.1	0.22	–	–	39.6	–	–
Pd/CZO Fresh	28.6	55.4	0.40	4.5	10.9	–	–	–
Pd/CZO Redox 700 °C/16 h	26.4	55.5	0.21	5.9	12.0	–	–	–

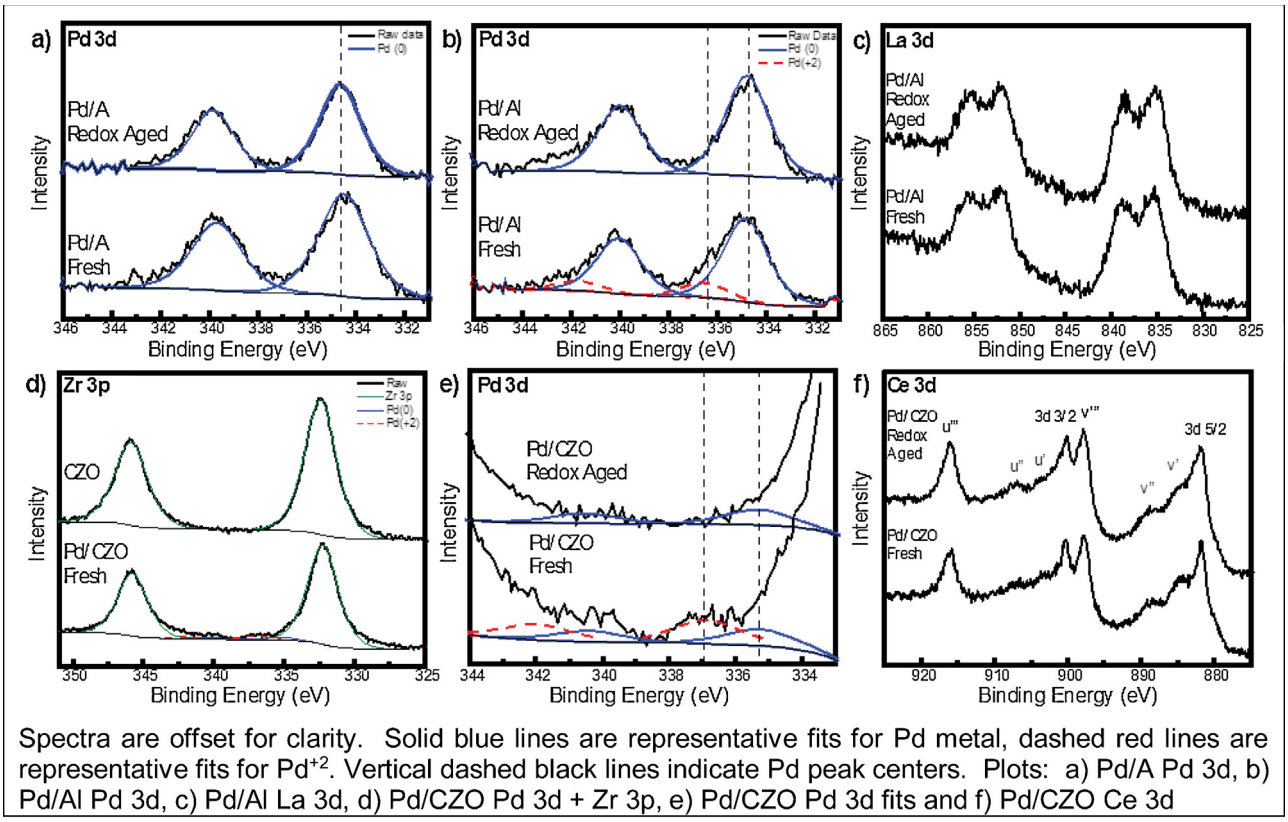

Spectra are offset for clarity. Solid blue lines are representative fits for Pd metal, dashed red lines are representative fits for Pd^{+2}. Vertical dashed black lines indicate Pd peak centers. Plots: a) Pd/A Pd 3d, b) Pd/Al Pd 3d, c) Pd/Al La 3d, d) Pd/CZO Pd 3d + Zr 3p, e) Pd/CZO Pd 3d fits and f) Pd/CZO Ce 3d

Fig. 5. XPS surface analysis of fresh and redox aged samples.

sity due to reducible oxides in the support [18,37,46,49]. However, the position of the Pd/A sample Pd metal peak is similar to that observed with the Pd/Al sample, in spite of the absence of La_2O_3. The Pd/Al sample La 3d peaks did not show a peak shift or change in intensity from the fresh to aged state.

The XPS spectra of the Pd/CZO catalyst samples are shown in Fig. 5, plots d–f. The Zr 3p plot of the reference CZO material compared to the Pd/CZO sample shows similar peak position. The Pd 3d peaks were fit inside the shoulders of the Zr 3p peaks. The fresh Pd/CZO sample had two Pd $3d_{5/2}$ peaks, a smaller one at 335.1 eV for Pd metal and a larger one at 336.9 eV for Pd^{+2}. While the fresh catalyst sample was reduced, about half of the fresh Pd was still Pd^{+2}, perhaps due to an abundance of interface sites with finely dispersed Pd and oxygen from CeO_2. These results are comparable to XPS work reported by Zhao et al. on fresh, reduced 1.4 wt% Pd on $Ce_{0.65}Zr_{0.30}La_{0.05}O_2$ support that had the Pd $3d_{5/2}$ peak at 335.9 eV, although no separate peaks of Pd^0 and Pd^{+2} were fitted [48]. The Pd metal peak location of Pd/CZO was 0.4 eV higher than Pd/Al and 0.6 eV higher than Pd/A. Redox aging of the Pd/CZO catalyst and accompanying coverage of Pd by CZO changed the Pd $3d_{5/2}$ peak location of Pd metal by +0.2 eV, but the Pd^{+2} peak was no longer observed. Alexandrou and Nix deposited CeO_2 on top of a Pd [111] single crystal substrate and observed a positive binding energy shift in the Pd $3d_{5/2}$ peak at 334.5 eV (clean) by about +2 eV with 3.8 mL of CeO_2, which was not reversed upon oxidation [35]. While Alexandrou and Nix ruled out Pd-Ce alloying [35], oxidation of metallic Pd interface sites by deposited CeO_2 may explain their observed positive binding energy shift. Since Fig. 5e shows minimal Pd peak shift with no Pd^{+2} peak after redox aging, the metallic Pd interface sites with oxygen supplied by CeO_2 were lost after coverage by Ce. The Pd/CZO sample Ce 3d peaks had a slight increase in intensity from the fresh to aged state, but the Ce $3d_{5/2}$ peak at 882.0 eV or the Ce $3d_{5/2}$ peak at 900.4 eV did not show a shift. The other Ce 3d peaks shown were satellite peaks that arose from interactions with the Ce 4f valence electrons after the 3d core electron was emitted. Each core level ($3d_{5/2}$ and $3d_{3/2}$) had 3 satellite peaks associated with it. The $3d_{5/2}$ satellite peaks were at v' = 884.0 eV, v'' = 889.1 eV, and v''' = 897.8 eV. Analogously, the $3d_{3/2}$ satellite peaks were at u' = 903.2 eV, u'' = 908.1 eV, and u''' = 916.3 eV.

3.5. Catalytic activity tests

The OSC and WGS tests were selected as probe reactions since these two CO conversion processes share the step of oxidation with potential spillover oxygen from the support. The oxidation of CO gives us insight into the contact between the noble metal and support at a given state of catalyst deterioration. These tests differ from CO oxidation light-off tests (co-feed of gas phase $CO + O_2$) since reaction with gas phase O_2 will confound metal-support O_2 mobility, and show performance trends essentially aligning with earlier Pd dispersion results and not providing new insight. All catalysts were initially in the reduced state prior to evaluation. CO and CO_2 was measured directly by a mass spectrometer in units of partial pressure (i.e, torr) and converted to concentration. Micromoles of CO_2 per gram of catalyst can be calculated for the OSC experiment using the following equation where the average CO_2 20 s before and after the CO pulse is used as the background:

$$\text{OSC } CO_2\left[\mu\text{moles/g}\right] = \frac{(\text{current } CO_2\,[\%] - \text{background } CO_2\,[\%]) \times (\text{CO pulse length}\,[\text{m}]) \times \left(\text{gas flow rate}\left[\text{L/m}\right]\right)}{22.414\text{L/mole} \times \text{mass of catalyst sample}\,[\text{g}]}$$

Conversion of CO to CO_2 during the WGS experiment can be calculated using the following equation where the aver-

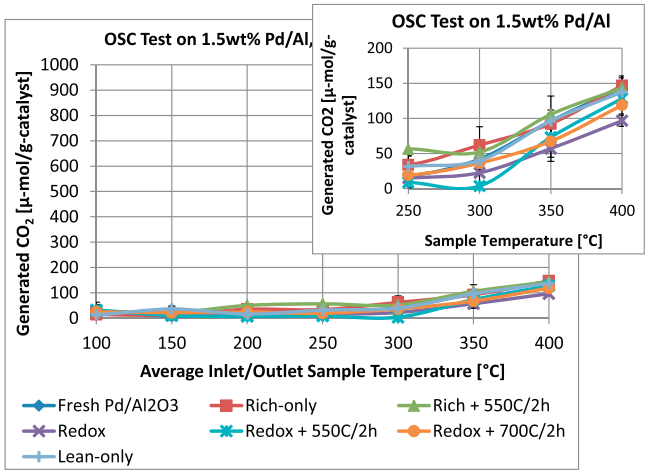

Fig. 6. Generated CO_2 over Pd/Al samples during OSC test.

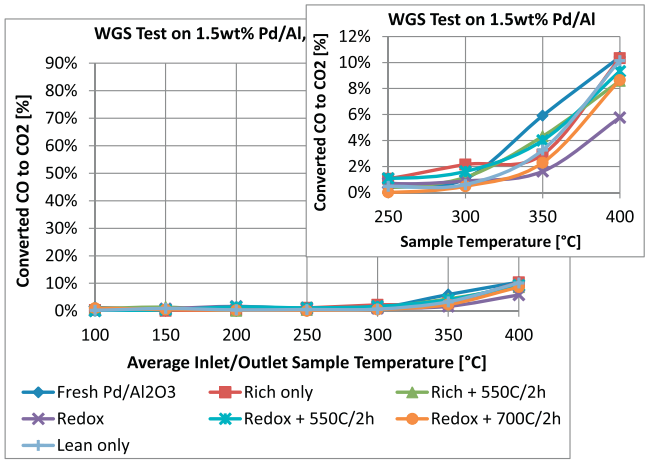

Fig. 7. CO conversion to CO_2 over Pd/Al samples during WGS test.

age CO_2 concentration at room temperature is used as a background:

$$\text{WGS conversion of CO to } CO_2\,[\%] = \frac{(\text{current } CO_2 - \text{background } CO_2)}{(\text{CO atroom temperature})}$$

The catalytic activity of Pd/Al samples measured by generation of CO_2 is shown in Fig. 6 for the OSC test and the conversion of CO to CO_2 is shown in in Fig. 7 for the WGS test. The trends observed for aging method severity at 400 °C were the same between the WGS and OSC and were as follows: redox > rich-only = lean-only. The amount of CO_2 generated during the OSC test was below 150 μmol CO_2/g and the CO_2 conversion on the WGS test was below 12%. The poor Pd/Al catalyst activity was due to the lack of oxygen mobility in the support material. CO_2 was generated in the lowest quantity over the redox aged sample compared to the other samples, and only significantly above 300 °C, likely due to the La_2O_3 interacting with Pd more after redox cycling than with a fixed rich-only environment. Both lean redispersion treatments showed a slight CO_2 generation benefit over the raw redox aged sample up to a comparable performance of the other samples. This suggests that 550 °C/2 h in air is sufficient to restore the chemical and geometric structure of Pd so that La_2O_3 does not inhibit CO adsorption on Pd/Al samples.

The catalytic activity of Pd/CZO samples measured by generation of CO_2 is shown in Fig. 8 for the OSC test and the conversion of CO to CO_2 is shown in Fig. 9 for the WGS test. The trends observed for aging method severity were the same between the WGS and

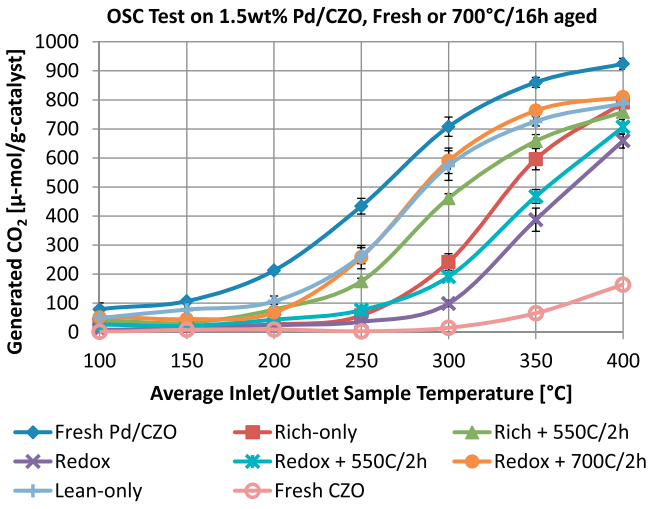

Fig. 8. Generated CO_2 over Pd/CZO samples during OSC test.

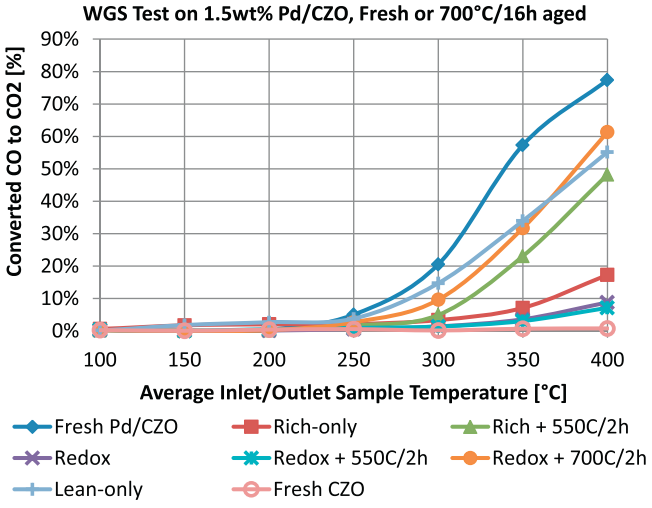

Fig. 9. CO conversion to CO_2 over Pd/CZO samples during WGS test.

OSC and were as follows: redox > rich-only » lean-only. These trends suggests that (1) redox aging brought more reducible oxide over the Pd surface than the fixed rich-only aging, (2) the reducible oxide on the Pd surface limited adsorption of CO for reaction with O_2, and (3) the interface sites between Pd and CZO with oxygen mobility were severely deactivated after redox aging. The 550 °C/2 h lean redispersion treatment showed a CO_2 generation benefit for the rich-only sample, but the redox sample showed only a slight improvement on the OSC test and no improvement for the WGS test. The 700 °C/2 h lean redispersion treatment showed a large benefit for the redox aged sample and improved the results to a level comparable with the lean-only aged sample for both tests. The uncatalyzed fresh CZO sample showed OSC activity comparable to the Pd/Al samples, illustrating the contribution of the CZO support towards CO adsorption and CO_2 generation. The uncatalyzed fresh CZO sample showed no WGS activity through 400 °C since this sample lacks the metal-support interface sites required for this reaction. The OSC data at 350 °C and 400 °C showed that the CO_2 conversion of the four most active catalysts were limited due to the complete consumption of CO over the first several seconds.

The catalytic activity of Pd/TWC samples measured by generation of CO_2 is shown in Fig. 10 for the OSC test and the conversion of CO to CO_2 is shown in Fig. 11 for the WGS test. The OSC test results appear to be simply an average of the results achieved with

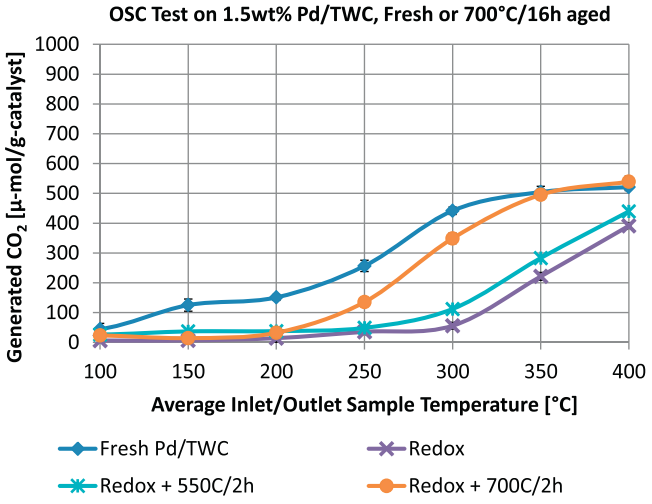

Fig. 10. Generated CO_2 over Pd/TWC samples during OSC test.

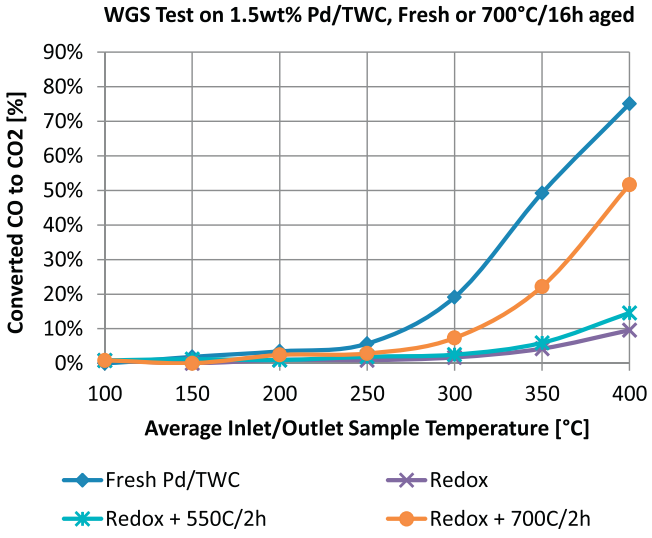

Fig. 11. CO conversion to CO_2 over Pd/TWC samples during WGS test.

the Pd/CZO and Pd/Al samples. The WGS test results appear to be comparable to the results achieved with the Pd/CZO sample. The 700 °C/2 h treatment in air showed significant improvement in the OSC and WGS performance over the redox aged sample while the 550 °C/2 h treatment in air showed perhaps a slight improvement.

The OSC and WGS mechanisms differ in how oxygen is supplied to the Pd. Three samples had undetectable Pd particles by H_2 chemisorption as listed in Table 2 that also showed the worst WGS and OSC performance, which suggest that these samples had Pd surfaces that were covered, perhaps by reducible Ce oxide separated from the CZO support. These "Ce-Pd/CZO" samples had WGS performance at 400 °C similar to the Pd/Al samples at 6-11% conversion of CO to CO_2, yet significantly lower than the other aged Pd/CZO samples at 47–62% conversion of CO to CO_2. For the Pd/Al and Ce-Pd/CZO samples to have the same WGS CO to CO_2 conversion, the CO and water should still adsorb onto the exposed surface of the Pd and perhaps the reducible Ce oxide decoration sites, but the mechanism for CZO support participation along the Pd-adlineation sites must be deactivated by the reducible Ce oxide decoration of Pd to render it essentially as inert as alumina. The reducible Ce oxide decoration seemed to block the sites necessary for oxygen, fed indirectly via water decomposition, to be fed to the Pd by the bulk CZO support along the adlineation sites. However the Ce-Pd/CZO samples were able to demonstrate OSC roughly 5 times greater than the Pd/Al samples and uncatalyzed CZO, but had much less OSC than the other Pd/CZO samples at 300 °C and lower. The CZO near the Pd particle may still supply limited oxygen, fed directly via gas phase adsorption, through the reducible Ce oxide that decorated and partially encapsulated the Pd.

A comparison of palladium on both supports was performed by normalizing the reaction rate to the accessible metal surface atoms. The CO_2 production rate for the WGS measurement was calculated using an equation from Han et al. where for a given temperature the turnover frequency (TOF) is the product of the following: the conversion of CO to CO_2 (X), the number of inlet CO molecules per second (dN_{CO}/dt) and divided by the number of exposed Pd surface atoms (N_S^{Pd}) [50]. The CO_2 production rate for the OSC measurement was calculated using a method from Hori et al. where the initial CO_2 generation peak edge was integrated during the CO pulse [51]. The event marker for $t_0 = 0$ was just before the CO_2 peak rise and the value of t_1 was at the maximum of the CO_2 peak or four seconds later for $t_1 = 4$.

CO_2 production rate as a turnover frequency:

$$\text{WGS : TOF}\left[1/s\right] = \left[\left(\frac{X}{100}\right) \times \left(\frac{dN_{co}}{dt}\right)\right] \times \left(\frac{1}{N_S^{Pd}}\right)$$

$$\text{OSC : TOF}\left[\frac{1}{s}\right] = \left[\frac{\int_{t_0}^{t_1} N_{CO_2}\,dt}{(t_1 - t_0)}\right] \times \left(\frac{1}{N_s^{Pd}}\right)$$

N_{CO} = Inlet molecules of CO per second

N_{CO_2} = Molecules of CO_2 formed

$$N_S^{Pd} = \frac{m_{cat} X_{Pd} D_{Pd} N_A}{M_{Pd}}$$

m_{cat} = Mass of catalyst [g]

X_{Pd} = Pd loading weight fraction

D_{Pd} = Pd dispersion by H_2 chemisorption

N_A = Avogadro's number

M_{Pd} = Pd molecularmass

The turnover frequencies (TOF) from the catalyst activity tests can be plotted in terms of the Arrhenius equation to determine the activation energy (E_a) and coefficient (A) as:

$$\text{In}(\text{TOF}) = \left(\frac{-E_a}{R}\right) - \left(\frac{1}{T}\right) + \text{In}(A)$$

Figs. 12 and 13 show the Arrhenius plots of catalyst activity. The WGS data used to plot the TOF ranged from 250 °C to 400 °C for both Pd/Al and Pd/CZO. The OSC data used to plot the TOF also ranged from 250 °C to 400 °C for Pd/Al, but only the data from 100 °C to 300 °C could be used for Pd/CZO to avoid the temperatures where the leading edge of inlet CO was completely consumed. The H_2 chemisorption technique was used to determine the Pd dispersion, since XRD could not detect a Pd peak for the fresh or lean-only aged samples. The Pd/Al samples each had a TOF that was similar to the others for the WGS and OSC tests; illustrating the contribution of the exposed Pd surface on a support without oxygen mobility. The Pd/CZO samples were each higher in TOF than the Pd/Al samples; the TOF gap illustrates the contribution of the support oxygen mobility and metal-support interface sites. The Pd/CZO samples

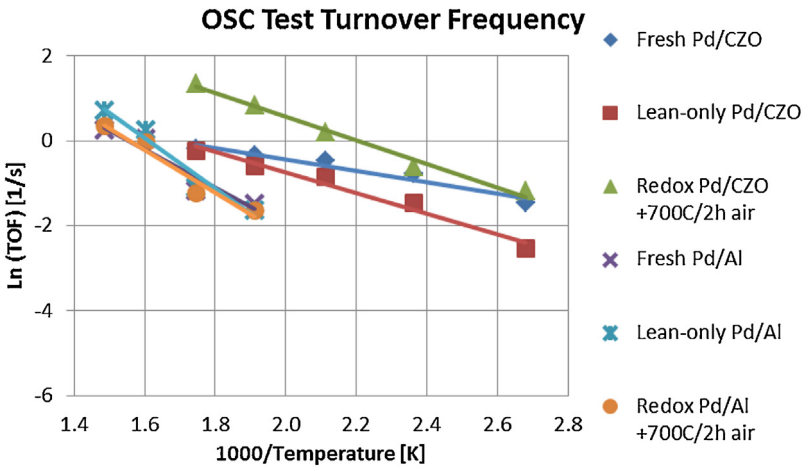

Fig. 12. Arrhenius plot of OSC test turnover frequency.

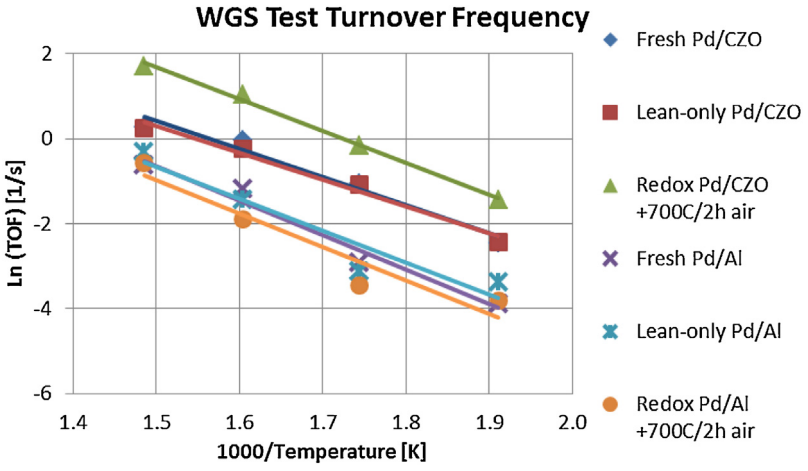

Fig. 13. Arrhenius plot of WGS test turnover frequency.

Table 5
Pd/CZO and Pd/Al kinetic parameters measured with OSC and WGS tests.

Catalyst sample	OSC test		WGS test	
	E_a (kJ/mol)	A	Ea (kJ/mol)	A
Pd/CZO fresh	11	9.5E+00	55	3.1E+04
Pd/CZO lean-only	20	6.0E+01	53	1.8E+04
Pd/CZO redox + 700C/2 h air	23	4.6E+02	63	2.9E+05
Pd/Al fresh	37	1.1E+03	68	1.1E+05
Pd/Al lean-only	49	1.4E+04	62	4.0E+04
Pd/Al redox + 700C/2 h air	42	2.6E+03	65	4.5E+04

also showed more separation in the TOF with the 700 °C/2 h air treated redox aged sample at a higher rate than the other samples for the WGS and OSC tests. An explanation for the higher apparent rate with the 700 °C/2 h air treated redox aged sample may be due to a higher participation of support sites near the Pd particles during the WGS and OSC tests. Support sites along the perimeter of the metal are called adlineation sites and on a reducible oxide are known to participate in catalytic activity tests [52]. The TOF equation contains an exposed Pd surface atoms term (N_S^{Pd}) that does not account for adlineation site participation from reducible oxides in the support. The composition of the metal-support interface sites were likely altered by the redox aging environment followed by reducible Ce oxide decomposition from the Pd surface during the 700 °C/2 h air treatment, enriching the local Pd interface sites with more CeO_2 than the original $Ce_{0.5}Zr_{0.5}O_2$ support of the fresh and lean aged samples. Other work with CZO solid solutions has shown available OSC was increased by over 20% when CeO_2 compositions were adjusted from 50% to 65% [53,54,55].

Table 5 lists the apparent E_a and A determined from linear fits of the Arrhenius equation in Figs. 12 and 13. The Pd/CZO samples had lower E_a than the Pd/Al samples in the OSC tests, demonstrating the benefit of support oxygen mobility on palladium CO oxidation. Therefore, CO oxidation appears to depend on the total number of metal-support interface sites and support oxygen transfer ability. The fresh samples from Table 5 are compared to similar fresh catalysts found in the literature as shown in Table 6 [50,56,57,58,59]. The WGS test in this work produced comparable E_a to the literature. The OSC rate calculation method from Hori et al. was used by others with an integration length convention set to one second ($t_1 = 1$) to calculate a so called dynamic oxygen storage capacity or rate (DOSC or DOSR) over a catalyst bed of 10 mm diameter by 1.5 mm long in a gas stream flowing at 300 mL/min [50,56]. Since they did not disclose an E_a, an Arrhenius equation fit was performed using their DOSC or DOSR test data provided from 200 °C to 500 °C to obtain the results listed in Table 6. The OSC test in this work produced a slightly higher E_a than the literature, which may be due to the difference in support ceria content or catalyst bed dimensions.

3.6. Examination for totally encapsulated palladium particles on ceria-zirconia

Characterization methods to determine whether aged Pd particles were completely encapsulated by the CZO support have been

Table 6
Comparison of TOF parameters to literature.

Fresh samples	E_a [kJ/mole]	ln A	Test	References
0.5 wt% $Pd/Ce_{0.67}Zr_{0.33}O_2$	28	6	WGS	[50]
1.8 wt% $Pd/Ce_{0.75}Zr_{0.25}O_2$	62	13.4	WGS	[57]
1.0 wt% $Pd/Ce_{0.5}Zr_{0.5}O_2$	49		WGS	[58]
1.5 wt% $Pd/Ce_{0.5}Zr_{0.5}O_2$	55	10	WGS	This work
1.8 wt% $Pd/Mg\text{-}Al_2O_3$	76	13.7	WGS	[57]
2.0 wt% Pd/Al_2O_3	82		WGS	[59]
1.5 wt% $Pd/La\text{-}Al_2O_3$	68	11.6	WGS	This work
0.5 wt% $Pd/Ce_{0.67}Zr_{0.33}O_2$	12	8	OSC	[50]
0.5 wt% $Pd/Ce_{0.7}Zr_{0.3}O_2$	6	8	OSC	[56]
1.5 wt% $Pd/Ce_{0.5}Zr_{0.5}O_2$	20	60	OSC	This work

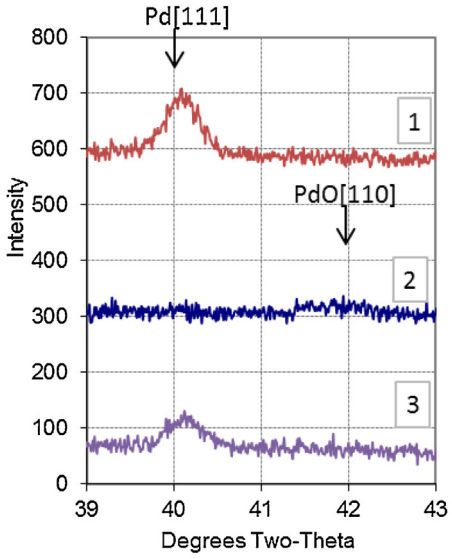

1. Redox aging was ended on rich step. Sample was cooled in N_2 then reduced at 350°C for 0.5h in 1% CO/H_2 balance N_2. Detectable Pd reduced to metal state.
2. Sample was then oxidized at 700°C for 2h in air. Detectable Pd was oxidized to PdO without showing encapsulated Pd metal at 40° 2θ.
3. Sample was then reduced at 350°C for 0.5h in 1% CO/H_2 balance N_2. Detectable Pd reduced to metal state.

Fig. 14. Examination for encapsulated Pd on CZO.

described in the scientific literature with similar catalysts. One method by Graham et al. involved a 2.25 wt% $Pd/Ce_{0.5}Zr_{0.5}O_2$ sample that was redox aged 1050 °C/12 h and later oxidized at 700 °C in air for 2 h where the XRD pattern showed both a strained Pd [111] peak at 40.5°2θ and the broad PdO [110] peak at 41.9° 2θ, which lead them to claim some Pd metal was inaccessible to the oxidation feed and must be buried by the CZO support as surface area was degraded by 97% [60].

Fig. 14 shows a similar sequence was applied to the 700 °C/16 h redox aged Pd/CZO sample in this study. Upon reoxidation at 700 °C for 2 h in step 2, the Pd [111] peak completely disappeared and a broad PdO [110] appeared just above the background. The lack of a clear PdO peak may indicate that the oxide is highly disordered perhaps even amorphous. So while the 700 °C/16 h redox aging condition caused a thin reducible Ce oxide layer to cover the Pd

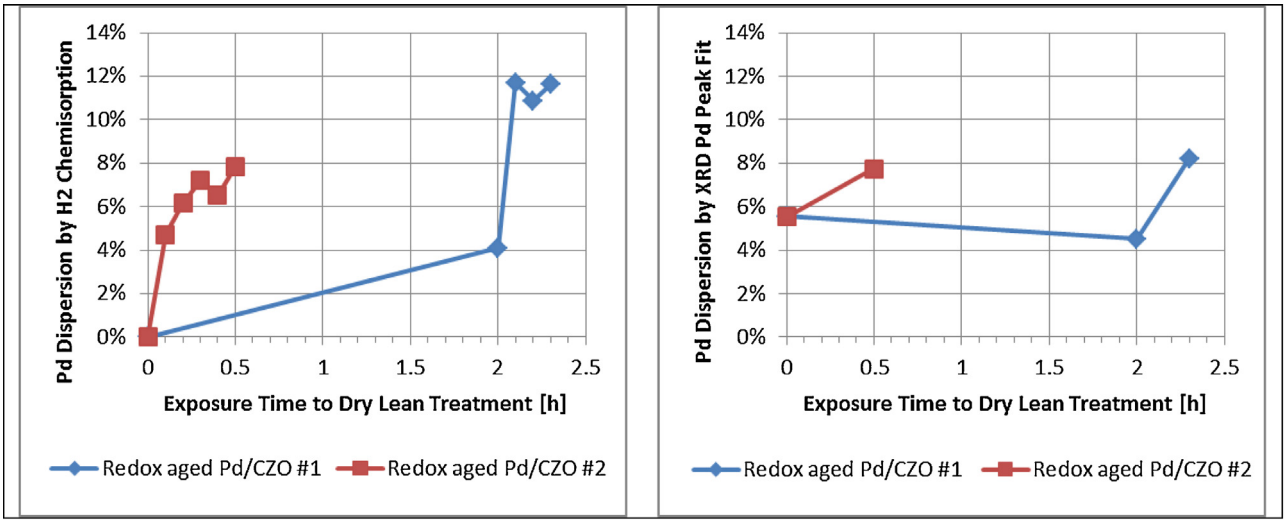

Fig. 15. Characterization of Pd/CZO after separate dry lean treatment schemes.

particles, gas phase oxygen decomposed the reducible Ce oxide and reoxidized the Pd metal.

Going from step 1 to step 3 it can be seen that the Pd [111] peak area decreased significantly. As shown previously in Table 2 for the effect of the 700 °C/2 h lean treatment, the XRD pattern Pd [111] peak fit resulted in a Pd size increase from 20 nm to 24 nm with an accompanying decrease in dispersion from 6% to 5%. However, the H_2 chemisorption results in Table 2 also showed an increase in Pd dispersion from u/d to 4%. A Pd dispersion increase measured by H_2 chemisorption without a corresponding decrease in Pd particle size as measured by XRD may be due to the following possibilities: (1) the lost Pd-CZO interface due to aging in a reducing environment (i.e., see Fig. 5e XPS plot of Pd^{+2} fresh to aged) was reestablished causing a significant portion of the Pd metal to go to PdO under the room temperature conditions, which is hard to observe at 41.9° 2θ apart from the background or (2) PdO particles actively redispersed to form new particles too small for XRD detection so that the peak width was due to just the particles larger than 7 nm.

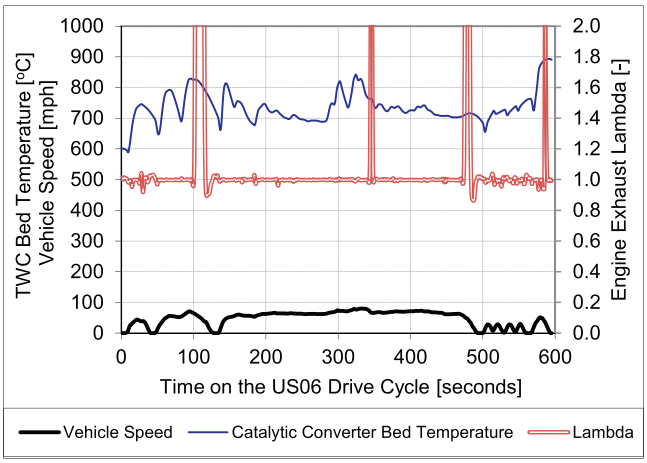

Fig. 16. Environment of a catalytic converter on the US06 drive cycle.

3.7. Investigation of the model for redispersed palladium particles on ceria-zirconia

An alternate lean/rich sequence was developed to gain further insight on the effects of a 700 °C lean treatment based on initially exposed Pd metal surface. The two portions of the Pd/CZO redox aged sample were selected with different Pd dispersion values determined by H_2 chemisorption: sample #1 was after the 700 °C/2 h lean treatment (4.1% dispersed Pd) and sample #2 was in as-is condition (no exposed Pd). Both samples were then exposed to repeated cycles of a brief 700 °C reoxidation in dry air for 0.10 h followed by the typical 350 °C reduction in pure H_2 for two hours as part of the automated H_2 chemisorption procedure. An XRD pattern was collected only after each sample reached the final lean/rich cycle.

Fig. 15 shows the Pd dispersion results by H_2 chemisorption after each lean/rich cycle. The two Pd/CZO redox aged samples achieved about the same level of apparent Pd dispersion in dry air at 700 °C with just 0.1 h as was achieved over two hours, which may be simply removal of Ce from the Pd surface. The Pd/CZO sample #1 with two hour lean treatment had an increase to the exposed Pd surface as measured by H_2 chemisorption yet no increase in bulk average Pd particle size as measured by XRD. If any PdO particles migrated and ruptured over those two hours, the new fragments were below the XRD detection limit and did not affect the bulk measurement. The following air treatment of 700 °C/0.1 h showed a dramatic increase in Pd dispersion to 12%, demonstrating that significant Pd redispersion was possible after the reducible Ce oxide covering was removed. Subsequent 700 °C/0.1 h air treatments showed no further improvements to Pd dispersion on Pd/CZO sample #1, but minor improvements to Pd dispersion were observed with Pd/CZO sample #2 to a cumulative total of 30 min with the Pd dispersion improved to 7.8% as measured by H_2 chemisorption. The improvements to Pd dispersion were confirmed with Pd size measurements by XRD then converted to dispersion; starting at a Pd crystallite size of 20 nm or 5.5% dispersion, the Pd on sample #1 shrank to 13 nm for 8.2% dispersion and the Pd on sample #2 shrank to 14 nm for 7.8% dispersion. Since both Pd/CZO samples ended with similar Pd size and dispersion by XRD, yet had different Pd dispersion by H_2 chemisorption, the discrepancy suggests that Pd/CZO sample #2 still had some reducible Ce oxide coverage on the Pd surface, causing only gradual improvement in Pd dispersion with each lean treatment. The 700 °C dry air treatment likely worked to reintegrate the decomposed reducible Ce oxide from the Pd surface into the phase segregated CZO, to a larger extent over two hours than in just 0.1 h. The surface of sample #2 was likely in a reversible state that allowed limited Ce creep over the Pd during each subsequent reduction in H_2 at 350 °C.

3.8. Comparison of lean Pd redispersion to vehicle exhaust conditions

So far we have looked at model catalysts under laboratory conditions. We now consider if these redispersion effects are consistent with conditions on a vehicle. A 2009MY 2.0L Ford Focus on gasoline fuel was driven at speeds from 0 to 80 mph while the catalytic converter bed temperature and exhaust gas equivalence lambda were acquired as shown in Fig. 16. The catalytic converter bed temperature reached temperatures in excess of 700 °C on multiple occasions when the vehicle speed was over 50 miles per hour. On a few of these occasions, the fuel was also shut off to the engine while the vehicle slowed down as shown when the engine exhaust lambda was in excess of 1. These events extended up to several seconds on the supplementary federal drive cycle US06. This confluence of air flowing through the engine for several seconds combined with a hot catalyst in excess of 700 °C should be similar to the dry lean Pd redispersion environments used in this study, although at a much shorter duration.

The model powder catalysts showed dynamic changes to Pd dispersion in the laboratory depending on oxygen concentration in the 700 °C aging environment for 16 h. The rich-only and redox environments caused much more severe loss of Pd dispersion than the fixed lean-only exhaust gas compositions, for both Pd/Al and Pd/CZO samples, producing samples with the lowest activity for the WGS and OSC tests. Exposure to dry air at 700 °C caused Pd particles to increase dispersion on alumina and CZO supports. Based on these observations made on the model catalysts and the environment shown in Fig. 16, one should operate the engine so that the exhaust gas composition falls along a trajectory that avoids the fuel-rich environment or includes periodic dry air events to reoxidize Pd into PdO to redisperse the Pd and restore lost activity. Automotive fuel-rich environments include fuel enrichment events commonly used to cool engine-out exhaust temperature and protect exhaust system components from thermal damage (i.e., catalyst protection). To maximize Pd dispersion on automotive catalysts either a lean exhaust environment or fuel cut event would be required prior to 16 h of 700 °C redox exhaust exposure or right after fuel enrichment events so that most of the Pd particles would be small enough to redisperse under moderate driving conditions. These conditions are achievable on a production vehicle and the fuel-cut frequency could be further enhanced through additional engine control features or parameter calibration refinement. Since this study evaluated a 16 h

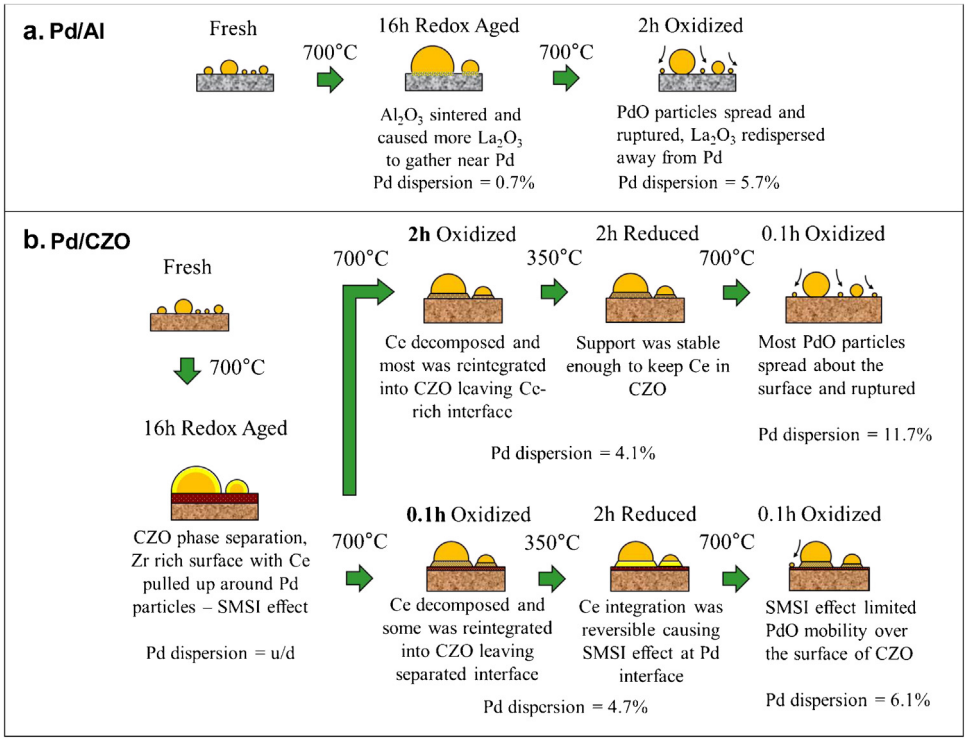

Fig. 17. Proposed Pd redispersion mechanism on Al and CZO Supports.

aging duration and lean Pd redispersion treatment at 2 h in length, further work will need to be done on measuring the time scales of Pd oxidation, redispersion and sintering. This appears to be a good strategy for maintaining adequate Pd dispersion on a catalytic converter under real-world driving conditions.

4. Discussion

4.1. Oxidation of the system, collapse of SMSI effect

Fig. 17a shows a proposed mechanism for the fresh Pd/Al redox aging, reoxidation and redispersion based on surface area, H_2 chemisorption, XPS, XRD and STEM results. The 16 h redox (and rich-only) aging environment sintered Al_2O_3 and increased La_2O_3 at the surface as measured by XPS, which caused the Pd/Al samples to have much larger Pd particle size measured by H_2 chemisorption than by XRD or STEM. To examine the SMSI effects caused by the La_2O_3 dopant, two alumina supports were used in this work, Pd/A was undoped while Pd/Al contained La_2O_3 and both had similar initial Pd dispersions. Comparing the redox aged Pd/Al and Pd/A samples showed a 7 fold difference in Pd diameter by H_2 chemisorption, yet the XRD method showed Pd particle diameters just 1 nm different from each other. This suggests that the reducing environment initiated an interaction between Pd and La_2O_3 in the Pd/Al sample that caused H_2 chemisorption to not accurately detect the exposed metal surface to provide a good estimation of Pd diameter. Comparing the redox aged Pd/Al samples before and after the 550 °C/2 h lean treatment, the H_2 chemisorption results showed the Pd particle shrank by over 5 fold, while the XRD and STEM methods showed the Pd particle size underwent a modest reduction. The oxidation of the system reversed the SMSI effects on Pd in the Pd/Al samples to enable improved gas phase adsorption onto Pd and a more accurate estimate of Pd size from H_2 chemisorption.

There is some debate in the literature as to how La_2O_3 affects Pd when exposed to high temperature reducing conditions. Rieck and Bell showed H_2 saturation coverage results on Pd/SiO_2 catalysts with an H atom coverage that diminished by half after it was promoted with 4 wt% La_2O_3, which they attributed to decoration of Pd particles by partially reduced LaO_x [19]. Ahn et al. used a H_2 temperature programmed reduction experiment with similar Pd catalysts to show a Pd reduction peak near 120 °C for all samples, plus an extra reduction peak near 320 °C with Pd/La_2O_3 and Pd/La_2O_3-SiO_2 catalysts, which they attributed to La_2O_3 reduction made possible by interaction with Pd [36]. However, others have concluded that the discrepancies with chemisorption on Pd-La_2O_3 catalysts stem from an electronegative shift of Pd shown by XPS [18], while others showed no change in the La^{+3} valence state after H_2 reduction at 600 °C [49]. Recently, Kim et al. furthered the work of Ahn et al. with Pd/SiO_2 and Pd/La_2O_3-SiO_2 catalysts, and concluded that the observed difference in the H_2 uptake from H_2 chemisorption coupled with an observed shift in Pd 3d electronic binding energy from XPS were both due to a change in the properties of Pd as influenced by the partially reduced La oxide, which lowered the adsorption strength of gas phase molecules onto the Pd surface [37]. Although La_2O_3 is claimed to be unreducible [18], in our work La_2O_3 caused the H_2 chemisorption measurement to underestimate the Pd/Al sample's Pd dispersion, relative to the Pd/A sample. The XPS results on the Pd/Al sample did not show decreased surface Pd coincident with the increased surface La after redox aging, so any coverage of Pd by La_2O_3 was ruled out in our case.

Fig. 17b shows a proposed mechanism for the fresh Pd/CZO redox aging, reoxidation and redispersion based on H_2 chemisorption, XPS, XRD, and normalized WGS and OSC results. The redox aging environment caused several changes: severe support sintering shown by dramatic BET surface area loss, no exposed Pd by H_2 chemisorption results, no Pd-support oxygen transfer by WGS activity tests and significantly increased surface Ce and Zr coupled with lowered surface Pd in our XPS results. Kępiński et al. used Pd supported on CeO_2 and claimed that thin films of reducible Ce oxide formed over Pd particles when reduced in hydrogen at 700 °C [20,34]. The Pd/CZO support used in this work contained

50% CeO_2, that once reduced is known to atomically migrate and decorate the surface of Pd particles [34], and creep up around the sides of Pd particles from the metal-support interface and cause partial encapsulation [33]. Taking all of these observations into contextual consideration, the best explanation is reducible ceria pulled from the Pd-CZO interface, decorated the Pd surface as a film. While these observations suggest a strong metal support interaction between ceria in CZO and the Pd interface during reducing conditions [20,33,34,38], we were unable to confirm this explanation with STEM images. We also could not confirm a CZO phase separation with the acquired XRD patterns, but a monolayer of Ce on the surface of Pd particles would not be detected by XRD. Because XRD involves constructive interference based on Bragg's Law, there have to be several layers of atoms for diffraction to occur. Even if the Ce was 3 or 4 atomic layers thick, the peak would be so broad and of low intensity (several degrees FWHM) that it would be lost in the background. In reality, a crystal needs to contain dozens or even hundreds of atom layers to be detected in powder XRD and even then significant peak broadening will be observed.

Post aging lean treatments appeared to reverse some of the reducible oxide effects, as evidenced by increased Pd dispersion and by increased CO_2 production during WGS and OSC activity measurements. There is precedent in the literature regarding why these Pd/CZO samples remained essentially unchanged after the 550 °C/2 h air treatment. Alexandrou and Nix deposited reducible Ce oxide films on a Pd [111] surface and heated it in N_2 under vacuum, then used XPS to show that Ce stayed on Pd relatively unchanged up to 500 °C, but then the Ce 3d peak dramatically dropped at 600 °C and completely vanished at 700 °C [35]. Badri et al. used diffuse reflectance infrared Fourier transform spectroscopy to show oxidation at 600 °C was sufficient to remove reducible Ce oxide decoration from the Pd [111] surface while the Pd [100] surface remained unchanged [38]. Dry air at 700 °C was a necessary first step to enable PdO mobility over the CZO support for redispersion, possibly by removal of a reducible ceria film decorated on the Pd surface or CZO from around the edges of the particle. The 700 °C/2 h air treatment enabled access for H_2 adsorption on the Pd surface, leading to better Pd dispersion agreement between H_2 chemisorption and XRD methods. The difference in Fig. 17b in initial lean treatment duration (0.1 h vs. 2 h) led to different CZO surfaces and degrees of uncoupled metal/support interaction. The smaller increase in Pd dispersion with the shorter air treatment duration is consistent with a lesser degree of reintegration of the film of reducible ceria into the bulk CZO. Until this process of reintegration is complete, the mobility of PdO may be restricted. The ceria-rich interface on the lean treated sample may be the reason that the normalized WGS and OSC reaction rates were higher than for the fresh condition.

4.2. Redispersion of Pd

To understand why Pd can redisperse rather than sinter at elevated temperatures it is important to remember that the oxygen concentration essentially governs whether Pd forms oxide particles or remains in the metallic phase. Our lean aging conditions had just 0.5% O_2, which was above the Pd decomposition line shown in Fig. 1. Gabasch et al. noted that PdO formation is kinetically limited near the decomposition temperature because the rate of PdO seeds formed at the onset of oxidation is comparable with the rate of PdO decomposition [61]. Therefore, in our lean-only aging condition, the Pd could not be sufficiently oxidized with 0.5% O_2 as the rate of PdO decomposition exceeded the rate of PdO seed formation. The Pd/Al catalysts sintered similarly in all three aging environments according to Pd size measurements by XRD, but the Pd/CZO catalysts were much less sintered in the lean-only environment than in the reducing aging environments suggesting enhanced PdO formation rates due to the support material. Our lean treatment conditions included 21% O_2 (air), which was well below the Pd decomposition line shown in Fig. 1. Collussi et al. showed that as gas phase oxygen concentration was increased from 0.5% to 21%, the onset temperature for supported PdO decomposition increased and the amount of O_2 uptake increased suggesting a more complete Pd reoxidation [17]. The kinetically limited conditions in the lean-only aging environment of 0.5% O_2 were reversed upon increasing to 21% O_2. The improved sintering resistance of PdO versus Pd under oxidizing conditions also relates to the difference in thermodynamic and physical properties of the metal and oxide. Recent microscopy and density functional theory work by Johns et al. showed that bulk PdO in air at 800 °C is very stable and does not emit atoms into the vapor phase (as by Ostwald ripening) [62]. Kang et al. aged Pd catalysts at 600 °C in 3–21% O_2 or 3% CO and showed a lower extent of Pd particle sintering that scaled with higher oxygen concentration [32]. The literature review conducted by Johns and Kang enabled them to link properties such as the roughly three orders of magnitude lower vapor pressure and 50% lower surface tension of PdO versus Pd metal as the reason behind the stability of the oxide [62,32]. Therefore, after the bulk oxide forms, the atomic Pd emission becomes more difficult, while PdO mobility and eventual fracture into smaller particles are enhanced.

The aftereffects of Pd redispersion was confirmed in this work through multiple Pd particle size estimation techniques with Pd/Al powder samples, before and after 550 °C or 700 °C dry lean treatments, where 700 °C showed more benefit than 550 °C for Pd size reduction. The proposed mechanism for Pd redispersion is consistent with microscopy observations from Chen and Ruckenstein where PdO crystallites moved about the film at 500 °C accompanied by rupturing and fracturing of the spreading PdO crystallites into smaller particles [11]. This mechanism is analogous to a reversed particle migration and coalescence sintering model requiring PdO mobility and sufficient time in the Pd redispersion zone shown in Fig. 1 to rupture into new PdO particles.

In this work, Pd particles were measured *ex-situ* on supported catalyst powder after exposure to air at 700 °C, holding for a fixed time and finally reducing in H_2 at 350 °C. We do not consider that the mild reduction at 350 °C in H_2 initiated a sloughing off of the oxide particle shell generating new Pd particles. Crozier et al. showed with high-resolution transmission electron microscopy on supported PdO exposed to H_2 from 200 °C to 550 °C that the final Pd particle size was not smaller than expected given the oxide removal and formation of an inner void space [41]. While the role of the reduction was important to enable a following Pd–PdO transformation, the new Pd particles that we observed *ex-situ* arose from the process of Pd oxidation, the ensuing PdO mobility, or both. Datye et al. observed that the process of Pd transformation into PdO alone did not cause Pd to redisperse on undoped alumina, according to their XPS and microscopy results on quenched sample portions taken during heating in air to 1000 °C then cooled in air to room temperature [63]. These results are consistent with recent work by Chen et al. who used a 550 °C dry lean treatment to achieve only modest Pd dispersion on variants of the undoped Pd/A sample used in this work [10]. Yet Peterson et al. showed that supported Pd clusters treated in air at 700 °C or with 1% O_2 achieved atomically dispersed Pd that was more stable on La-Al_2O_3 than on undoped alumina [64]. The observations of Peterson et al. also are consistent with our XPS results where Pd^{+2} was observed on the fresh Pd/Al and Pd/CZO samples, but not on the fresh Pd/A sample, which were all calcined then later reduced prior to analysis. The ability of Pd to form stable Pd^{+2} on the surface of La-Al_2O_3 or CZO may be vital to achieving significant Pd size reduction when inside the conditions of the Pd redispersion zone.

5. Conclusions

The three catalyst aging environments used in this study at 700 °C for 16 h produced Pd/CZO samples with distinct levels of residual surface area, Pd particle size and WGS/OSC activity. A ranking relative to the aging environment severity on these samples was as follows: redox > rich-only » lean-only. The Pd particle size and WGS/OSC activity differences for the aged Pd/Al samples had similar trends, but were much smaller in magnitude, and even showed no significant difference in the residual surface area across the aging environments than the Pd/CZO samples. Therefore different aging protocols can to lead to very different catalyst structures and performance characteristics through a combination of metal oxidation state effects and support/additive interactions.

The fresh and lean-only aged Pd/CZO samples had exposed Pd particles measurable by H_2 chemisorption, while the rich-only and redox samples did not. The Pd/CZO samples with the highest dispersion had the highest CO oxidation in the OSC and WGS activity tests. Therefore, CO oxidation by support oxygen transfer appears to depend on the Pd dispersion, which correlates to the total number of metal-support interface sites. However, the lean treatments of 700 °C after redox aging and 550 °C after rich-only aging produced Pd/CZO samples that did not agree with this conclusion, demonstrating high catalyst activity with low Pd dispersion.

HAADF STEM images of Pd/Al redox aged samples confirmed the effects of dry air treatments on Pd particle size. The 550 °C/2 h lean treatment produced a 1.4 nm decrease in the mean Pd size with no increase in the fraction of particles at 10 nm and below, yet the large particles at 30 nm to 80 nm shrank down from 5% of the aged total to 1%. The 550 °C in air treatment shrank the particles of 16 nm and higher, increasing the count of particles measuring 11–15 nm from 36% to 43% of the total. The 700 °C/2 h lean treatment produced a 4.4 nm decrease in the mean Pd size with a near doubling of the fraction of aged particles at 10 nm and below, confirming the significance of Pd redispersion under these conditions.

The 700 °C lean treatment was confirmed to redisperse Pd on La-Al_2O_3, but on CZO the results were mixed. The reducing aging environment brought more La and Ce oxide to the surface from the support as measured by XPS, which showed no change in surface Pd on La-Al_2O_3, but caused a loss of half the surface Pd on CZO. The initial lean treatment on the redox aged Pd/CZO increased the exposed Pd surface as measured by H_2 chemisorption, perhaps by decomposition of decorated Ce from Pd, but the Pd crystal size was not diminished as measured by XRD. The next lean treatment showed a large improvement in Pd dispersion, as measured by both XRD and H_2 chemisorption, almost up to the lean-only aged sample. Since Pd redispersion appears to require PdO mobility, lean treatments via engine fuel cuts need to be applied before reducible oxides creep up and restrain the Pd metal or multiple lean treatments would be needed in close succession.

The insights gained from this study provide important guidance into the operation of a catalytic converter on a vehicle. The engine exhaust environment capable of redispersing palladium catalyst particles seems to be aligned with fuel cuts during a deceleration event from high vehicle speed. If the catalyst is properly positioned near the engine exhaust manifold, then the temperature may be above the threshold of 700 °C when air would be pumped through the engine on a fuel cut. The automotive catalytic converter could then be periodically regenerated with active engine controls to prolong the performance throughout the life of the catalyst. The result of this work may enable lower initial amounts of noble metals in the catalytic converter if the dispersion can be maintained above 1% by full useful life.

Acknowledgements

The authors gratefully acknowledge the following sources of funding for this study: Ford University Research Program (URP), NSF GOALI grant # CBET-1159279 and NSF grant # DMR-9871177. The authors thank Dr. William Paxton at Ford Motor Company for valuable discussions regarding artifacts in XRD patterns of Pd/CZO.

References

[1] H.S. Gandhi, G.W. Graham, R.W. McCabe, Automotive exhaust catalysis, J. Catal. 216 (2003) 433–442.
[2] J. Kašpar, P. Fornasiero, N. Hickey, Automotive catalytic converters: current status and some perspectives, Catal. Today 77 (2003) 419–449.
[3] R.M. Heck, R.J. Farrauto, Automobile exhaust catalysts, Appl. Catal. A: Gen. 221 (2001) 443–457.
[4] C. Bartholomew, Mechanisms of catalyst deactivation, Appl. Catal. A: Gen. 212 (2001) 17–60.
[5] A. Datye, Q. Xu, K. Kharas, J. McCarty, Particle size distributions in heterogeneous catalysts: what do they tell us about the sintering mechanism? Catal. Today 111 (2006) 59–67.
[6] R. Goeke, A. Datye, Model oxide supports for studies of catalyst sintering at elevated temperatures, Top. Catal. 46 (2007) 3–9.
[7] R. McCabe, R. Useman, Characterization of Pd-based automotive catalysts, Stud. Surf. Sci. Catal. 101 (1996) 355–368.
[8] Q. Xu, K. Kharas, B. Croley, A. Datye, The sintering of supported Pd automotive catalysts, ChemCatChem 3 (2011) 1004–1014.
[9] N. Hickey, P. Fornasiero, R. Di Monte, J. Kašpar, J.R. González-Velasco, M.A. Gutiérrez-Ortiz, M.P. González-Marcos, J.M. Gatica, S. Bernal, Reactivation of aged model Pd/$Ce_{0.68}Zr_{0.32}O_2$ three-way catalyst by high temperature oxidising treatment, Chem. Commun. 1 (2004) 196–197.
[10] X. Chen, Y. Cheng, C.Y. Seo, J.W. Schwank, R.W. McCabe, Aging, re-dispersion, and catalytic oxidation characteristics of model Pd/Al_2O_3 automotive three-way catalysts, Appl. Catal. B: Environ. 163 (2015) 499–509.
[11] J.J. Chen, E. Ruckenstein, Role of interfacial phenomena in the behavior of alumina-supported palladium crystallites in oxygen, J. Phys. Chem. 85 (1981) 1606–1612.
[12] N.M. Rodriguez, S.G. Oh, R.A. Dalla-Betta, R.T.K. Baker, In-situ electron microscopy studies of palladium supported on Al_2O_3, SiO_2, and ZrO_2 in oxygen, J. Catal. 157 (1995) 676–686.
[13] E. Ruckenstein, J.J. Chen, Wetting phenomena during alternating heating in O_2 and H_2 of supported metal crystallites, J. Coll. Interface Sci. 86 (1982) 1–11.
[14] H. Lieske, J. Völter, Pd redispersion by spreading of PdO in O_2 treated Pd/Al_2O_3, J. Phys. Chem. 89 (1985) 1841–1842.
[15] R.J. Farrauto, J.K. Lampert, M.C. Hobson, E.M. Waterman, Thermal decomposition and reformation of PdO catalysts; support effects, Appl. Catal. B: Environ. 6 (1995) 263–270.
[16] M. Peuckert, XPS study on surface and bulk palladium oxide, its thermal stability, and a comparison with other noble metal oxides, J. Phys. Chem. 89 (1985) 2481–2486.
[17] S. Colussi, A. Trovarelli, E. Vesselli, A. Baraldi, G. Comelli, G. Groppi, J. Llorca, Structure and morphology of Pd/Al_2O_3 and Pd/CeO_2/Al_2O_3 combustion catalysts in Pd–PdO transformation hysteresis, Appl. Catal. A: Gen. 390 (2010) 1–10.
[18] R.F. Hicks, Q.-J. Yen, A.T. Bell, Effects of metal-support interactions on the chemisorption of H_2 and CO on Pd/SiO_2 and Pd/La_2O_3, J. Catal. 89 (1984) 498–510.
[19] J.S. Rieck, A.T. Bell, Studies of the interactions of H_2 and CO with Pd/SiO_2 promoted with La_2O_3, CeO_2, Pr_6O_{11}, Nd_2O_3, and Sm_2O_3, J. Catal. 99 (1986) 278–292.
[20] L. Kępiński, M. Wolcyrz, J. Okal, Effect of chlorine on microstructure and activity of Pd/CeO_2 catalysts, J. Chem. Soc. Farad. Trans. 91 (1995) 507–515.
[21] J.C. Jiang, X.Q. Pan, G.W. Graham, R.W. McCabe, J. Schwank, Microstructure of a Pd/ceria-zirconia catalyst after high-temperature aging, Catal. Lett. 53 (1998) 37–42.
[22] D. Briggs, M.P. Seah, Practical Surface Science Analysis by Auger and X-ray Photoelectron Spectroscopy, John Wiley & Sons, New York, 1984.
[23] A.L. Patterson, The Scherrer formula for X-ray particle size determination, Phys. Rev. 56 (1939) 978–982.
[24] J.E. Benson, H.S. Hwang, M. Boudart, Hydrogen–oxygen titration method for the measurement of supported palladium surface areas, J. Catal. 30 (1973) 146–153.
[25] V. Ragaini, R. Giannantonio, P. Magni, L. Lucarelli, G. Leofanti, Dispersion measurement by the single introduction method coupled with the back-sorption procedure: a chemisorption and TPD study of the different chemisorbed hydrogen species II. Pd on alumina, J. Catal. 146 (1994) 116–125.
[26] T. Takeguchi, S. Manabe, R. Kikuchi, K. Eguchi, T. Kanazawa, S. Matsumoto, W. Ueda, Determination of dispersion of precious metals on CeO_2-containing supports, Appl. Catal. A: Gen. 293 (2005) 91–96.
[27] D. Bresenham, J. Reisel, K. Neusen, Spindt air-fuel ratio method generalization for oxygenated fuels, Soc. Automot. Eng. SP-1381 (1998) 219–238.

[28] A. Baylet, S. Royer, P. Marécot, J. Tatibouët, D. Duprez, Effect of Pd precursor salt on the activity and stability of Pd-doped hexaaluminate catalysts for the CH_4 catalytic combustion, Appl. Catal. B: Environ. 81 (2008) 88–96.
[29] S. Meriani, Features of the caeria-zirconia system, Mat. Sci. Eng. A109 (1989) 121–130.
[30] S. Suhonen, M. Valdin, M. Hietikko, R. Laitinen, A. Savimäki, M. Härkönen, Effect of Ce–Zr mixed oxides on the chemical state of Rh in alumina supported automotive exhaust catalysts studied by XPS and XRD, Appl. Catal. A: Gen. 218 (2001) 151–160.
[31] I. Heo, J.W. Choung, P.S. Kim, I.S. Nam, Y.I. Song, C.B. In, G.K. Yeo, The alteration of the performance of field- aged Pd- based TWCs towards CO and C_3H_6 oxidation, Appl. Catal. B: Environ 92 (2009) 114–125.
[32] S.B. Kang, S.J. Han, S.B. Nam, I.S. Nam, B.K. Cho, C.H. Kim, S.H. Oh, Effect of aging atmosphere on thermal sintering of modern commercial TWCs, Top. Catal. 56 (2013) 298–305.
[33] H.P. Sun, X.P. Pan, G.W. Graham, H.-W. Jen, R.W. McCabe, S. Thevuthasan, C.H.F. Peden, Partial encapsulation of Pd particles by reduced ceria-zirconia, Appl. Phys. Lett. 87 (2005) 201915.
[34] L. Kępiński, M. Wolcyrz, Microstructure of Pd/CeO_2 catalyst: effect of high temperature reduction in hydrogen, Appl. Catal. A: Gen. 150 (1997) 197–220.
[35] M. Alexandrou, R.M. Nix, The growth, structure and stability of ceria overlayers on Pd(111), Surf. Sci. 321 (1994) 47–57.
[36] I.Y. Ahn, W.J. Kim, S.H. Moon, Performance of La_2O_3- or Nb_2O_5-added Pd/SiO_2 Catal. in acetylene hydrogenation, Appl. Catal. A: Gen. 308 (2006) 75–81.
[37] E. Kim, E.W. Shin, C.W. Bark, I. Chang, W.J. Yoon, W.-J. Kim, Pd catalyst promoted by two metal oxides with different reducibilities: Properties and performance in the selective hydrogenation of acetylene, Appl. Catal. A: Gen. 471 (2014) 80–83.
[38] A. Badri, C. Binet, J.-C. Lavalley, Metal-support interaction in Pd/CeO_2 catalysis Part 2. Ceria textural effects, J. Chem. Soc. Farad. Trans. 92 (9) (1996) 1603–1608.
[39] L.F. Allard, E. Voelkl, D.S. Kalakkad, A.K. Datye, Electron holography reveals the internal structure of palladium nano-particles, J. Mat. Sci. 29 (1994) 5612–5614.
[40] F.J. Cadete Santos Aires, R. Darji, J.F. Trillat, A. Howie, A. Renoprez, Hollow metallic particles obtained by oxidation/reduction treatment of organometallic precursors, Stud. Surf. Sci. Catal. 130 (2000) 1109–1114.
[41] P.A. Crozier, A.K. Datye, Direct observation of reduction of PdO to Pd metal by in situ electron microscopy, Stud. Surf. Sci. Catal. 130 (2000) 3119–3124.
[42] J. Railsback, A. Johnston-Peck, J. Wang, J. Tracy, Size-dependent nanoscale kirkendall effect during the oxidation of nickel nanoparticles, ACS Nano 4 (2010) 1913–1920.
[43] Y. Yin, R. Rioux, C. Erdonmez, S. Hughes, G. Somorjai, P. Alivisatos, Formation of hollow nanocrystals through the nanoscale kirkendall effect, Science 304 (2004) 711–714.
[44] A.J. Hayter, Probability and Statistics for Engineers and Scientists, PWS Publishing Co., Boston, MA, 1996.
[45] C.R. Adams, H.A. Benesi, R.M. Curtis, R.G. Meisenheimer, Particle size determination of supported catalytic metals: platinum on silica gel, J. Catal. 1 (1962) 336–344.
[46] T.H. Fleisch, R.F. Hicks, A.T. Bell, X.P.S. An, Study of metal-support interactions on Pd/SiO_2 and Pd/La_2O_3, J. Catal. 87 (1984) 398–413.
[47] J.S. Rieck, A.T. Bell, Studies on the interactions of H_2 and CO with silica- and lanthana-supported palladium, J. Catal. 96 (1985) 88–105.
[48] M. Zhao, X. Li, L. Zhang, C. Zhang, M. Gong, Y. Chen, Catalytic decomposition of methanol to carbon monoxide and hydrogen over palladium supported on $Ce_{0.65}Zr_{0.30}La_{0.05}O_2$ and La-Al_2O_3, Catal. Today 175 (2011) 430–434.
[49] M. Shelef, L.P. Haack, R.E. Soltis, J.E. deVries, E.M. Logothetis, An XPS study of interactions in thin films containing a noble metal with valence-invariant and reducible oxides, J. Catal. 137 (1992) 114–126.
[50] Z. Han, J. Wang, H. Yan, J. Fan, Performance of dynamic oxygen storage capacity, water–gas shift and steam reforming reactions over Pd-only three-way catalysts, Catal. Today 158 (2010) 481–489.
[51] C. Hori, A. Brenner, S. Ng, K. Rahmoeller, D. Belton, Studies of the oxygen release reaction in the platinum-ceria-zirconia system, Catal. Today 50 (1999) 299–308.
[52] K. Hayek, R. Kramer, Z. Paál, Metal-support boundary sites in catalysts, Appl. Catal. A: Gen. 162 (1997) 1–15.
[53] Y. Madier, C. Descorme, A.M. Le Govic, D. Duprez, Oxygen mobility in CeO_2 and $Ce_xZr_{(1-x)}O_2$ compounds: study by CO transient oxidation and $^{18}O/^{16}O$ isotopic exchange, J. Phys. Chem. B 103 (1999) 10999–11006.
[54] A. Trovarelli, F. Zamar, J. Llorca, C. de Leitenburg, G. Dolcetti, J.T. Kiss, Nanophase fluorite-structured CeO_2–ZrO_2 catalysts prepared by high-energy mechanical milling: analysis of low-temperature redox activity and oxygen storage capacity, J. Catal. 169 (1997) 490–502.
[55] J.-P. Cuif, G. Blanchard, O. Touret, A. Seigneurin, M. Marczi, E. Quéméré, (Ce, Zr)O_2 solid solutions for three-way catalysts, Soc. Automot. Eng. SP-288 (1997) 35–47.
[56] M. Yang, M. Shen, J. Wang, J. Wen, M. Zhao, J. Wang, W. Wang, Pd-supported interaction-defined selective redox activities in Pd-Ce0.7Zr0.3O2-Al2O3 model three-way catalysts, J. Phys. Chem. C 113 (2009) 12778–12789.
[57] A. Boisen, T.V.W. Janssens, N. Schumacher, I. Chorkendorff, S. Dahl, Support effects and catalytic trends for water gas shift activity of transition metals, J. Mol. Catal. A: Chem. 315 (2010) 163–170.
[58] S. Zhao, R.J. Gorte, The activity of Fe–Pd alloys for the water–gas shift reaction, Catal. Lett. 92 (2004) 75–80.
[59] L. Bollmann, J.L. Ratts, A.M. Joshi, W.D. Williams, J. Pazminoa, Y.V. Joshi, J.T. Miller, A.J. Kropf, W.N. Delgass, F.H. Ribeiro, Effect of Zn addition on the water–gas shift reaction over supported palladium catalysts, J. Catal. 257 (2008) 43–54.
[60] G. Graham, H. Jen, W. Chun, R. McCabe, Encapsulation of Pd particles by ceria-zirconia mixed oxides, Catal. Lett. 44 (1997) 185–187.
[61] H. Gabasch, W. Unterberger, K. Hayek, B. Klötzer, E. Kleimenov, D. Teschner, S. Zafeiratos, M. Hävecker, A. Knop-Gericke, R. Schlögl, J. Han, F.H. Ribeiro, B. Aszalos-Kiss, T. Curtin, D. Zemlyanov, In situ XPS study of Pd(111) oxidation at elevated pressure, Part 2: palladium oxidation in the 10^{-1} mbar range, Surf. Sci. 600 (2006) 2980–2989.
[62] T.R. Johns, R.S. Goeke, V. Ashbacher, P.C. Thüne, J.W. Niemantsverdriet, B. Kiefer, C.H. Kim, M.P. Balogh, A.K. Datye, Relating adatom emission to improved durability of Pt–Pd diesel oxidation catalysts, J. Catal. 328 (2015) 151–164.
[63] A.K. Datye, J. Bravo, T.R. Nelson, P. Atanasova, M. Lyubovsky, L. Pfefferle, Catalyst microstructure and methane oxidation reactivity during the Pd–PdO transformation on alumina supports, Appl. Catal. A: Gen. 198 (2000) 179–196.
[64] E.T. Peterson, A.T. DeLaRiva, S. Lin, R.S. Johnson, H. Guo, J.T. Miller, J.H. Kwak, C.H.F. Peden, B. Kiefer, L.F. Allard, F.H. Ribeiro, A.K. Datye, Low-temperature carbon monoxide oxidation catalysed by regenerable atomically dispersed palladium on alumina, Nat. Commun. 5 (2014) 4885.